12-1988

A Volume Integral Formulation for Electromagnetic Scattering from Homogeneous Dielectric Bodies

Mark Joseph Povinelli
Syracuse University

A VOLUME INTEGRAL FORMULATION FOR ELECTROMAGNETIC SCATTERING FROM HOMOGENEOUS DIELECTRIC BODIES

by

Mark Joseph Povinelli

B.S., University of Houston, 1982

THESIS

Submitted in partial fulfillment of the requirements for the
degree of Master of Science in Electrical Engineering
in the Graduate School of Syracuse University
December 1988

Approved R. F. Harrington

Date Dec. 16, 1988

ACKNOWLEDGEMENTS

The author wishes to express his appreciation and sincere gratitude to his advisor, Professor Roger F. Harrington, for his guidance, patience, and help in this work. He is indebted to Professor Ercument Arvas for time and energy spent discussing this work and for his comparative numerical results from the surface equivalence formulation. He is also grateful for the suggestions and comments from Dr. Joseph R. Mautz. The author extends his appreciation to Professor Arlon T. Adams for his teaching and serving as a member of the examining committee.

TABLE OF CONTENTS

LIST OF FIGURES

LIST OF FIGURES (Continued)

1.0 INTRODUCTION

In recent years, printed circuit antennas have become very useful in conformal and planar phased array antenna systems. Of particular interest is the radiation and scattering performance of stripline and microstrip printed circuit antenna array–elements used in these systems. These elements are generally made up of a complex three–dimensional distribution of dielectrics and conductors, which can include microstrip or stripline feed circuitry on a dielectric substrate. Figure 1 shows the geometry of a typical multilayer printed circuit stripline–fed flared slot antenna, used as an array–element in a multioctave planar phased array antenna. This antenna element design also incorporates a stripline to slotline coupling transition through the dielectric layers which further increases the intricacy of the near fields. An explicit model of these types of complicated printed circuit geometries is needed for predicting their radiation and scattering characteristics. A numerical method that utilizes a digital computer to subdivide the composite three–dimensional geometry and to organize the associated computations would be beneficial. This is especially important when one considers the larger problem of modeling arrays of multiple antenna elements and the environment surrounding the antenna (i.e., radomes, ground planes, and absorbers).

In this work, a numerical technique is developed to solve for the electromagnetic field scattered from the dielectric substrate portion of the printed circuit problem. The near electric field of a dielectric body is primarily produced by the bound charge residing on the surface. An accurate model of the near field is obtained through the use of this bound charge density in an integral formulation. A method of moments solution technique is used to numerically solve for the scattered field [1]. This solution approach should also yield a reliable prediction of the radiated fields for the antenna problem when extended to modeling the full problem of conductors on the dielectric substrate.

A number of approaches to modeling dielectric bodies involving polarization currents in a volume integral formulation have been developed for solving the electromagnetic scattering problem. Earlier work on scattering by dielectric bodies, which considered the volume currents that generate the scattered field, includes that given by Cohen in 1955 [2]. This work applied the reaction concept to calculate the scattered field from a dielectric circular cylinder. A transverse magnetic (TM) wave and a transverse electric (TE) wave scattering solution for dielectric cylinders of an arbitrary cross–section were presented by Richmond [3, 4] in 1965 and 1966, respectively. For TM wave scattering, the volume current was expanded in pulses and approximated by a uniform distribution over the square subsections used to model the cross–sectional area. In the TE wave scattering solution, the volume current was expanded in pulses and the associated charge was approximated by a sinusoidal distribution over a cylindrical perimeter bounding a cross–sectional area equal to the square subsection. A formulation using tetrahedral modeling for computing the electromagnetic scattered field from arbitrarily shaped inhomogeneous dielectric bodies was given by Schaubert, Wilton, and Glisson [5]. In this formulation the volume charge density was not explicitly constrained to be zero in the piecewise homogeneous dielectric volume of the body. A numerical solution of TE scattering by arbitrarily shaped two–dimensional composite bodies (dielectrics and conductors), subdivided into triangular regions of polarization current, was presented by Langan and Wilton [6]. Similarly, this approach did not specifically enforce the equa-

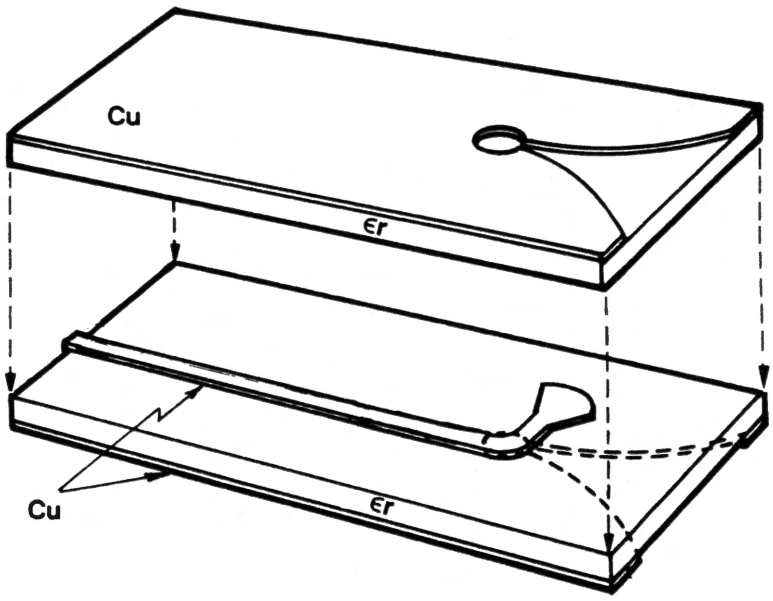

Figure 1. Stripline–Fed Flared Slot (Notch) Antenna Element

tion of continuity in the homogeneous portion of the material body. Both of these methods also required the solution of an integro–differential equation where the current was expressed in terms of electric flux density. The differentiation in the volume formulation for the tetrahedral modeling case was approximated by assuming the scalar potential varied slowly, so that it's derivative could be replaced by the value at the centroid of the tetrahedron. Evaluation of the derivatives in the scalar potential term for the two–dimensional composite bodies was solved in a similar manner by taking the average value over the line segment or triangular region as the value at the centroid.

More recently, a volume integral formulation for two–dimensional TE wave and three–dimensional electromagnetic wave scattering from thin dielectric substrates was presented by Povinelli and Harrington, using square cell divisions and a small cubic cell, while satisfying the equation of continuity in the homogeneous medium [7]. In this formulation, an integral equation was obtained where differentiation in the scalar potential term was avoided by applying a vector identity, the equation of continuity (enforcement of all volume charge density to be zero), and the divergence theorem. This work presents the formulation and numerical solution of scattering from two– and three–dimensional homogeneous dielectric bodies similar to the work given in [7]. The equation of continuity is imposed to insure that no volume charge density exists within the body. This reduces the electric scalar potential term, originally involving both a volume and surface integral, to purely a surface integral. The proper choice of current expansions constrains the charge to the surface, where volume polarization currents terminate in surface charge. This results in a more precise representation of the surface charge density than was given by Richmond in [4]. By reducing the equation obtained in the volume integral formulation to one entailing integration only, all divergent integrals are avoided. The moment matrix solution from this formulation yields accurate results with relatively few unknowns (expansion functions) as compared to other numerical solutions. Computer solutions of bistatic scattering cross section from two– and three–dimensional dielectric bodies are used to compare this volume integral formulation to a surface equivalence formulation for various square cell and subsectional approximations.

The volume integral formulation for two– and three–dimensional bodies is given in Section 2.0. For three–dimensional problems, the magnetic vector potential is expressed as a volume integral, and the electric scalar potential term is reduced to a surface integral. For two–dimensional problems, the vector potential is a surface integral and the scalar potential term is a line integral. An impedance operator is written, which relates the scattered field to the polarization currents. An operator equation is then formulated for the current with the incident field as the known. In Section 3.0 a method of moments solution to the operator equation derived in Section 2.0 is formulated. These matrix equations are in terms of unknown volume polarization current expansion coefficients. The matrix equation is written in terms of a modified impedance operator which includes vector potential, scalar potential and displacement current terms. The method of moments procedure is used where the testing functions are chosen to be equal to the basis (or expansion) functions. The unknown expansion functions are defined in Section 4.0 as circulating current loops. These current expansions are given as constant expansions in $\underline{u}_x$, $\underline{u}_y$, and $\underline{u}_z$ for the three–dimensional solution, and as rooftop functions in the two–dimensional solution. Evaluation of the matrix elements and the numerical results for bistatic TE scattering from two–dimensional models are given in Section 5.0. To simplify the vector potential integrals, a pulse

approximation to the rooftop functions is used and the second integrations are approximated by evaluating the integrand at the center of the cell. Examples of computed results from models using the volume integral formulation are compared to other numerical computations.

In Section 6.0 the matrix elements are evaluated and the numerical results are given for bistatic electromagnetic scattering from a homogeneous dielectric cube. An approximate solution using a few unknowns (one expansion per dimension) is compared to results from a surface equivalence formulation.

The conclusions and recommendations of this study are given in Section 7.0. Future research to enhance the accuracy of the three–dimensional solution is outlined. In Appendices A and C, the bistatic radar cross section equation is developed for two– and three–dimensions. Appendix B gives the evaluation of a two–dimensional surface integral for the scalar potential term in the three–dimensional formulation.

2.0 THE VOLUME INTEGRAL FORMULATION

The volume integral formulation can be used to determine the electromagnetic scattered field in the presence of a dielectric body [1]. In this section an impedance operator is derived which relates the scattered field to the induced polarization current. An operator equation is written using the impedance operator and the displacement current expression in terms of a known incident field. Only the time–harmonic case is considered, with $e^{j\omega t}$ time dependence suppressed, resulting in complex equations.

2.1 Statement of the Problem

Consider an electric field $\underline{E}^i$ incident upon a homogeneous material body of volume V, as shown in Figure 2. The homogeneous body has a relative permittivity of ϵ_r bounded by a surface S. The total electric field $\underline{E}$ in the presence of the body is given by

$$\underline{E} = \underline{E}^i + \underline{E}^s \tag{2.1}$$

which is the summation of both the incident field $\underline{E}^i$ and the scattered field $\underline{E}^s$. The impressed field $\underline{E}^i$ produces polarization current in the homogeneous dielectric body. This induced volume polarization current produces a scattered field $\underline{E}^s$. The final polarization current $\underline{J}$ depends on the total electric field $\underline{E}$, including the field contribution from the dielectric body. Within the dielectric material body the polarization current is given by

$$\underline{J} = j\omega(\epsilon - \epsilon_o)\,\underline{E} = j\omega(\epsilon - \epsilon_o)\,(\underline{E}^i + \underline{E}^s) \tag{2.2}$$

This is the (macroscopic) polarization current which arises in the body due to the motion of bound charges initially caused by the impressed incident electric field. The permittivity of the material is defined as the product of ϵ_o (permittivity of free–space) and the relative permittivity (dielectric constant) ϵ_r.

$$\epsilon = \epsilon_r \epsilon_o \tag{2.3}$$

Rearrangement of (2.2) yields

$$\underline{E}^i = \frac{\underline{J}}{j\omega(\epsilon - \epsilon_o)} - \underline{E}^s \tag{2.4}$$

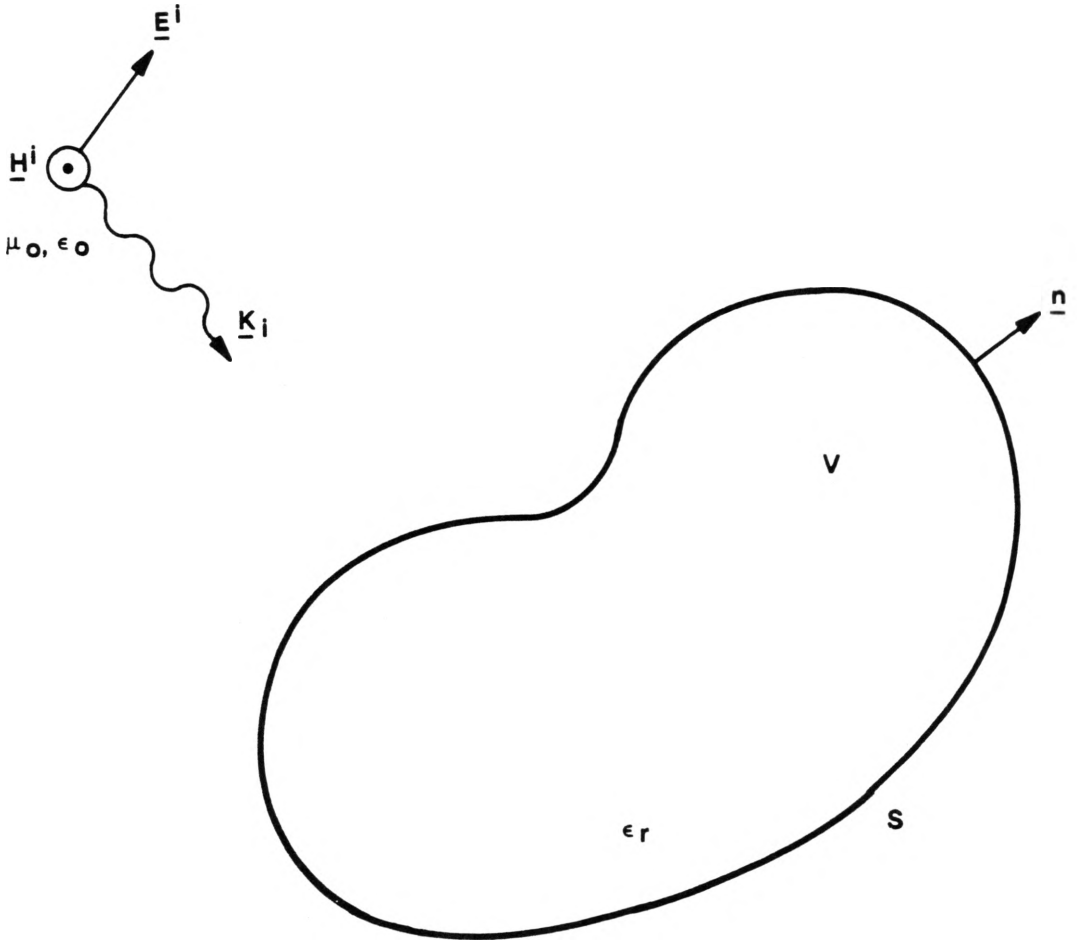

Figure 2. Homogeneous Material Body in the Presence of an Electromagnetic Incident Field

2.2 Derivation of the Operator Equation

The scattered field $\underline{E}^s$ produced by the polarization current can be written in terms of a magnetic vector potential $\underline{A}$ and an electric scalar potential ϕ as

$$\underline{E}^s = -j\omega\underline{A} - \nabla\phi \tag{2.5}$$

The magnetic vector potential and the electric scalar potential can be expressed as a superposition of sources [8] or they can be obtained by applying Green's theorem to the Helmholtz wave equation. The magnetic vector potential is written in terms of $\underline{J}$ as

$$\underline{A}(\underline{J}) = \mu_o \iiint_V \underline{J}(\underline{r}')\, G(\underline{r},\underline{r}')\, dv' \tag{2.6}$$

The electric scalar potential from an inhomogeneous dielectric body is written in terms of the volume polarization current $\underline{J}$ through a surface charge density ($\sigma = \frac{1}{j\omega}\, \underline{J} \cdot \underline{n}$) integral and a volume charge density ($q = -\frac{1}{j\omega}\, \nabla \cdot \underline{J}$) integral. The general scalar potential is then

$$\phi\ (\sigma, q) = \frac{1}{\epsilon_o} \left\{ \iint_S \sigma(\underline{r}')\, G(\underline{r},\underline{r}')\, ds' + \iiint_V q(\underline{r}')\, G(\underline{r},\underline{r}')\, dv' \right\} \tag{2.7}$$

For three-dimensional problems the free-space Green's function $G(\underline{r},\underline{r}')$ is

$$G(\underline{r},\underline{r}') = \frac{e^{-jk|\underline{r} - \underline{r}'|}}{4\pi\ |\underline{r} - \underline{r}'|} \tag{2.8}$$

where $G(\underline{r},\underline{r}')$ represents a three-dimensional field at $\underline{r}$ due to a source at $\underline{r}'$. The wave number $k = \omega \sqrt{\mu_o \epsilon_o} = 2\pi/\lambda$ where λ is the free space wavelength and ϵ_o, μ_o are the permittivity and permeability of the surrounding medium.

For two-dimensional problems, the vector potential integral in (2.6) becomes a surface integral and the scalar potential integrals in (2.7) involve a line integral and a surface integral. The Green's function is represented in terms of a zero order Hankel function of the second kind as

$$G(\underline{\rho},\underline{\rho}') = \frac{1}{4j}\, H_o^{(2)}\ (k\ |\underline{\rho} - \underline{\rho}'|) \tag{2.9}$$

where $\underline{\rho}$ is the two-dimensional radius vector to the field point and $\underline{\rho}'$ is the radius vector to the source point.

The volume charge density q for a homogeneous dielectric body in an incident electric field is zero

$$\underline{\nabla} \cdot \underline{J} = -j\omega q(\underline{r}') = j\omega(\epsilon - \epsilon_o)\, \underline{\nabla} \cdot \underline{E} = 0 \tag{2.10}$$

since all the microscopic dipole moments are equal, and within the macroscopic volume all the negative and positive charges cancel. This is explicit from Maxwell's equations where the divergence of the curl of the magnetic field is zero. These electric dipole moment orientations are not specifically defined since the spatial location of each atom or molecule in the material is not fixed. The zero divergence of the volume current directly specifies that all bound charge density resides on the surfaces in an impressed electric field. This can be observed from the physical picture of dipoles of charge aligned to produce zero bound volume charge density (cancellation of inner charges) resulting in uncancelled outer bound charge residing on the surface.

From the relationship established between charge and potential, the potential due to a homogeneous dielectric material arises from the charge distribution (bound charge density σ) on the surface (similar to the electrostatic case [9]). By relating the surface charge to the volume current terminating at the surface of the dielectric, an accurate representation of the near and far electric fields can be obtained. This model of the volume polarization current and surface charge density relationship has rarely been used in the literature.

The surface charge density σ in the scalar equation (2.7) is related to the volume polarization current in the body according to

$$\sigma = \frac{1}{j\omega}\, \underline{n} \cdot \underline{J} \tag{2.11}$$

where $\underline{n}$ is the unit normal to the surface S and $\underline{n} \cdot \underline{J}$ represents the normal component of $\underline{J}$ at the dielectric surface. This derivation of the surface charge density for the dynamic case is similar to the relationship in the static field case [10]. Since the divergence of the polarization current in the volume is zero, the resulting electric scalar potential equation involves only a surface integration. (This result is also obtained from the physical picture relating unbalanced polarization current in the material to surface charge density). The scalar potential integral in (2.7) is now only a function of bound charge density on the surface, (caused by the dipole moment in the material) given by

$$\phi(\sigma) = \frac{1}{\epsilon_o} \iint_S \sigma(\underline{r}')\, G(\underline{r},\underline{r}')\, ds' \tag{2.12}$$

This is the specialized electric scalar potential integral for homogeneous material bodies.

An impedance operator Z is defined which relates $\underline{E}^s$ to $\underline{J}$ (in 2.5) by

$$Z(\underline{J}) = -\underline{E}^s = j\omega \underline{A}(\underline{J}) + \nabla\phi(\sigma) \tag{2.13}$$

Substitution of this expression into (2.4) results in the operator equation

$$Z(\underline{J}) + \frac{\underline{J}}{j\omega(\epsilon - \epsilon_o)} = \underline{E}^i \qquad \text{in V} \tag{2.14}$$

This integro–differential equation can be solved using a method of moments solution technique to determine the electromagnetic field in a homogeneous dielectric media. The integro–differential operator is reduced to a pure integral operator in Section 3. The vector potential is obtained by integrating over the dielectric body V and the scalar potential term is obtained by integrating over the dielectric surface S. For the two–dimensional case the vector potential is obtained by integrating over the dielectric cross–section and the scalar potential is obtained by integrating over the boundary line segments of the cross–section.

3.0 METHOD OF MOMENTS SOLUTION

In this section, the method of moments is used to reduce the integro–differential equation (2.14) to a matrix equation. The integro–differential impedance matrix operator is further reduced to a matrix operator involving only integration. The polarization current $\underline{J}$ is expanded in terms of divergence free expansion functions. These functions must be chosen to produce no volume distribution of charge and a surface distribution of charge where they have a normal component at the surface. The choice of expansion functions will assure that all improper integrals are convergent.

3.1 Moment Matrix Formulation

The moment method is applied by choosing expansion functions $\underline{J}_n$ to approximate the volume current $\underline{J}$ in (2.14) by

$$\underline{J} = \sum_{n=1}^{N} I_n \underline{J}_n \tag{3.1}$$

(where $\underline{J}_n$ satisfies (2.10) in the homogeneous volume) and the surface charge σ in (2.14), defined for each $\underline{J}_n$ through (2.11), is given by

$$\sigma = \frac{1}{j\omega} \sum_{n=1}^{N} I_n \underline{n} \cdot \underline{J}_n \tag{3.2}$$

over the boundary. In these two expressions the I_n's are complex constants with n = 1, 2, ... N, where N is the total number of current expansions defined in the body. Equations (3.1) and (3.2) are substituted into (2.6) and (2.12), where the impedance operator $Z(\underline{J})$ is obtained through evaluation of (2.13). The approximated polarization current $\underline{J}$ in (3.1) is also substituted into (2.14) for the displacement current expression $\frac{\underline{J}}{j\omega(\epsilon - \epsilon_o)}$. Using the linearity of Z the integro–differential equation (2.14) can then be written in terms of the basis functions as

$$\sum_{n=1}^{N} I_n \left[Z(\underline{J}_n) + \frac{\underline{J}_n}{j\omega(\epsilon - \epsilon_o)} \right] = \underline{E}^i \qquad \text{in V} \tag{3.3}$$

A symmetric product for the solution of the problem is defined by

$$\langle A, B \rangle = \iiint_V \underline{A} \cdot \underline{B} \, dv \tag{3.4}$$

where $\underline{A}$ and $\underline{B}$ are two vector functions defined in V. A Galerkin type method is used for testing the moment solution, where the testing functions are defined as

$$\underline{J}_m = \underline{J}_n \qquad m = 1, 2, \ldots N \tag{3.5}$$

The symmetric product of (3.3) is taken with each $\underline{J}_m$ yielding,

$$\sum_{n=1}^{N} I_n \left\langle \underline{J}_m, Z(\underline{J}_n) + \frac{\underline{J}_n}{j\omega(\epsilon - \epsilon_o)} \right\rangle = \langle \underline{J}_m, \underline{E}^i \rangle \tag{3.6}$$

This set of equations can be written in matrix form as

$$[Z_{mn}][I_n] + \frac{[\hat{S}_{mn}][I_n]}{j\omega(\epsilon - \epsilon_o)} = [V_m^i] \tag{3.7}$$

where $[I_n]$ represents the unknown current expansion coefficients, $[V_m^i]$ is the known incident field (voltage) matrix with elements

$$V_m^i = \langle \underline{J}_m, \underline{E}^i \rangle \tag{3.8}$$

$[\hat{S}_{mn}]$ is the Gram matrix of the current expansions with elements

$$\hat{S}_{mn} = \langle \underline{J}_m, \underline{J}_n \rangle \tag{3.9}$$

and $[Z_{mn}]$ is the impedance matrix with elements

$$Z_{mn} = \langle \underline{J}_m, Z(\underline{J}_n) \rangle \tag{3.10}$$

These impedance matrix elements are written in expanded form as

$$Z_{mn} = \iiint_V \underline{J}_m \cdot (j\omega \underline{A}_n + \nabla \phi_n)\, dv \tag{3.11}$$

where $\underline{A}_n = \underline{A}\,(\underline{J}_n)$, and $\phi_n = \phi\,(\sigma_n)$. The surface charge density is related to the expansion current by

$$\sigma_n = \frac{1}{j\omega}\, \underline{n} \cdot \underline{J}_n \tag{3.12}$$

The impedance elements involve a volume integration of both the vector potential term and the gradient of a scalar potential term. This integro–differential operator can be refined to terms involving only integration.

3.2 Formulation of Matrix Integral Elements

The differentiation in equation (3.11) can be reduced to integration avoiding the highly singular nature of the electric field near the surface charge. These matrix elements are then directly relatable to integrable current and charge [11]. The vector identity

$$\nabla \cdot (\underline{J}\phi) = \underline{J} \cdot \nabla\phi + (\nabla \cdot \underline{J})\phi \tag{3.13}$$

is applied to (3.11) to give

$$Z_{mn} = \iiint_V \{j\omega\, \underline{J}_m \cdot \underline{A}_n + \nabla \cdot (\underline{J}_m\, \phi_n) - (\nabla \cdot \underline{J}_m)\, \phi_n\}\, dv \tag{3.14}$$

Relating the volume charge density and current through the equation of continuity

$$\nabla \cdot \underline{J}_m = -j\omega q_m \tag{3.15}$$

and then substituting (3.15) into (3.14),

$$Z_{mn} = \iiint_V \{j\omega\, \underline{J}_m \cdot \underline{A}_n + \nabla \cdot (\underline{J}_m\, \phi_n) - (-j\omega q_m\, \phi_n)\}\, dv \tag{3.16}$$

Next the divergence theorem

$$\iiint_V \nabla \cdot \underline{F} \, dv = \iint_S \underline{F} \cdot \underline{n} \, ds \tag{3.17}$$

is applied to (3.16) resulting in

$$Z_{mn} = \iiint_V \{j\omega \underline{J}_m \cdot \underline{A}_n + j\omega q_m \phi_n\} \, dv + \iint_S \underline{n} \cdot \underline{J}_m \phi_n \, ds \tag{3.18}$$

and noting that all the volume charge is equal to zero in the homogeneous volume (i.e., $\nabla \cdot \underline{J}_m = -j\omega q_m = 0$) an equation involving integration alone is obtained

$$Z_{mn} = \iiint_V j\omega \underline{J}_m \cdot \underline{A}_n \, dv + \iint_S \underline{n} \cdot \underline{J}_m \phi_n \, ds \tag{3.19}$$

This is the general equation for computing the impedance matrix elements with no differentiation.

3.3 Numerical Solution of the Operator Equation

The impedance integral operator (3.19) can be rewritten as a modified impedance operator by including the displacement current term defined (in matrix form) by

$$[S_{mn}] = \frac{[\hat{S}_{mn}]}{j\omega(\epsilon - \epsilon_o)} \tag{3.20}$$

as

$$[\hat{Z}_{mn}] = [VP_{mn}] + [SP_{mn}] + [S_{mn}] \tag{3.21}$$

where $\hat{S}_{mn}$ is given by (3.9).

In this equation VP_{mn} are the vector potential element terms, SP_{mn} are the scalar potential elements, and S_{mn} are the displacement current terms for two- and three-dimensional problems. The modified impedance equation for computation of the matrix elements for three-dimensional problems is defined by

$$\hat{Z}_{mn} = j\omega \iiint_V \underline{J}_m \cdot \underline{A}_n \, dv + \iint_S \underline{n} \cdot \underline{J}_m \, \phi_n \, ds + \frac{1}{j\omega(\epsilon - \epsilon_o)} \iiint_V \underline{J}_m \cdot \underline{J}_n \, dv \tag{3.22}$$

where

$$\underline{A}_n = \underline{A}(\underline{J}_n) = \frac{\mu_o}{4\pi} \iiint_V \underline{J}_n(\underline{r}') \frac{e^{-jk|\underline{r} - \underline{r}'|}}{|\underline{r} - \underline{r}'|} \, dv' \tag{3.23}$$

and

$$\phi_n = \phi(\sigma_n) = \frac{1}{4\pi\epsilon_o} \iint_S \sigma_n(\underline{r}') \frac{e^{-jk|\underline{r} - \underline{r}'|}}{|\underline{r} - \underline{r}'|} \, ds' \tag{3.24}$$

and for two-dimensional problems as

$$\hat{Z}_{mn} = j\omega \iint_S \underline{J}_m \cdot \underline{A}_n \, ds + \int_\ell \underline{n} \cdot \underline{J}_m \, \phi_n \, d\ell + \frac{1}{j\omega(\epsilon - \epsilon_o)} \iint_S \underline{J}_m \cdot \underline{J}_n \, ds \tag{3.25}$$

where

$$\underline{A}_n = \underline{A}(\underline{J}_n) = \frac{\mu_o}{4j} \iint_S \underline{J}_n(\underline{\rho}') \, H_o^{(2)} \, (k \, |\underline{\rho} - \underline{\rho}'|) \, ds' \tag{3.26}$$

and

$$\phi_n = \phi(\sigma_n) = \frac{1}{4j\epsilon_o} \int_\ell \sigma_n(\underline{\rho}') \, H_o^{(2)} \, (k \, |\underline{\rho} - \underline{\rho}'|) \, d\ell' \tag{3.27}$$

The matrix equation (3.7) can now be written in terms of the modified impedance operators $\hat{Z}_{mn}$ as

$$[\hat{Z}_{mn}][I_n] = [V_m^i] \tag{3.28}$$

The solution for the expansion coefficients can be found by rearranging (3.28) as

$$[I_n] = [Y_{mn}][V_m^i] \tag{3.29}$$

where

$$[Y_{mn}] = [\hat{Z}_{mn}^{-1}] \tag{3.30}$$

is the modified admittance matrix. The computational solution depends on choosing appropriate expansion functions $\underline{J}_n$ and accurately evaluating the modified impedance matrix elements.

4.0 DEVELOPMENT OF EXPANSION FUNCTIONS

The matrix equation (3.29) can be used to solve for the expansion coefficients in two– and three–dimensional problems, with the proper choice of expansion functions that satisfy the equation of continuity within V.

4.1 Three–Dimensional Expansion Model

The electric dipole moment orientations in the dielectric body are not specifically defined; therefore, a simple $\underline{u}_x$, $\underline{u}_y$, and $\underline{u}_z$ orientation of circulating polarization current loops is adopted. The circulating current, shown in Figure 3, terminates in a surface charge density doublet for all unbalanced (partial) current loops. In this analysis the three–dimensional volume is modeled by cubic cells. The simplest three–dimensional current expansions for one cell would be a constant expansion in $\underline{u}_x$, $\underline{u}_y$, and $\underline{u}_z$ through the volume terminating in surface charge at the centroids of each face of the cube.

4.2 Two–Dimensional Expansion Model

For two–dimensional problems the circulating current loops are defined in the cross–sectional area as depicted in Figure 4. These current loops are oriented in the $\underline{u}_x$ and $\underline{u}_y$ directions as illustrated in Figure 5 with partial current loops terminating in surface charge at the dielectric boundary. The cross–sectional area is modeled using a total number of N square cells as shown in Figure 6 with four quarter components of current $\underline{J}_n$ defined in a cell–wise basis. The depicted area (modeled with cells) has full and partial (quarter–, half–, and three–quarter) circulating current loops, dependent on the number of cells used and their geometrical orientations. Each $\underline{u}_x$ and $\underline{u}_y$ component of expansion current $\underline{J}_n$ exists over the entire cell in which it is defined. The partial current loops terminate in surface charge over the cell boundaries in which they exist.

To simplify evaluation of the vector potential and scalar potential terms the source and field points for the current and charge are located at the centroid of the respective cells or cell sides as shown in Figure 7. Located at the midpoint of an exterior cell boundary ℓ_i (in which the polarization current terminates) are the surface charge density source and field points where i denotes which exposed exterior boundary of a cell is being evaluated. The local coordinates representation for self term ($\underline{J}_n = \underline{J}_m$) surface charges is also shown in Figure 7. A linear combination of rooftop functions [12, 13] can be used as expansion functions to approximate these full and partial circulating currents while satisfying the equation of continuity in the homogeneous volume.

The magnitude of a half rooftop function is defined as a right triangular function of x (or y) times a pulse function of y (or x) (i.e., T(x)P(y) or T(y)P(x)). The triangular function is further specified along the direction of current flow and the pulse function is in the orthogonal direction.

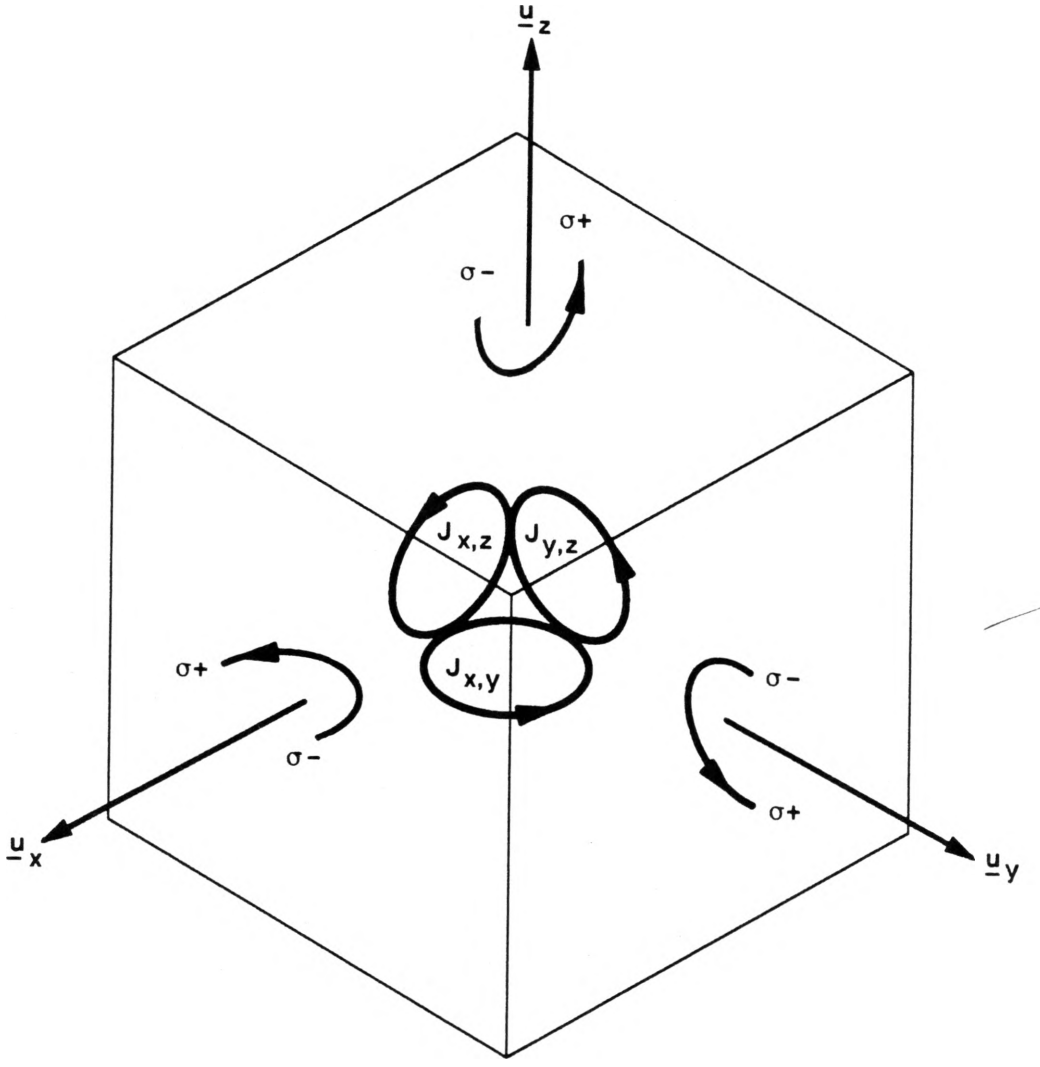

Figure 3. Circulating Volume Polarization Current Loops and Surface Charge Doublets

Fig 1

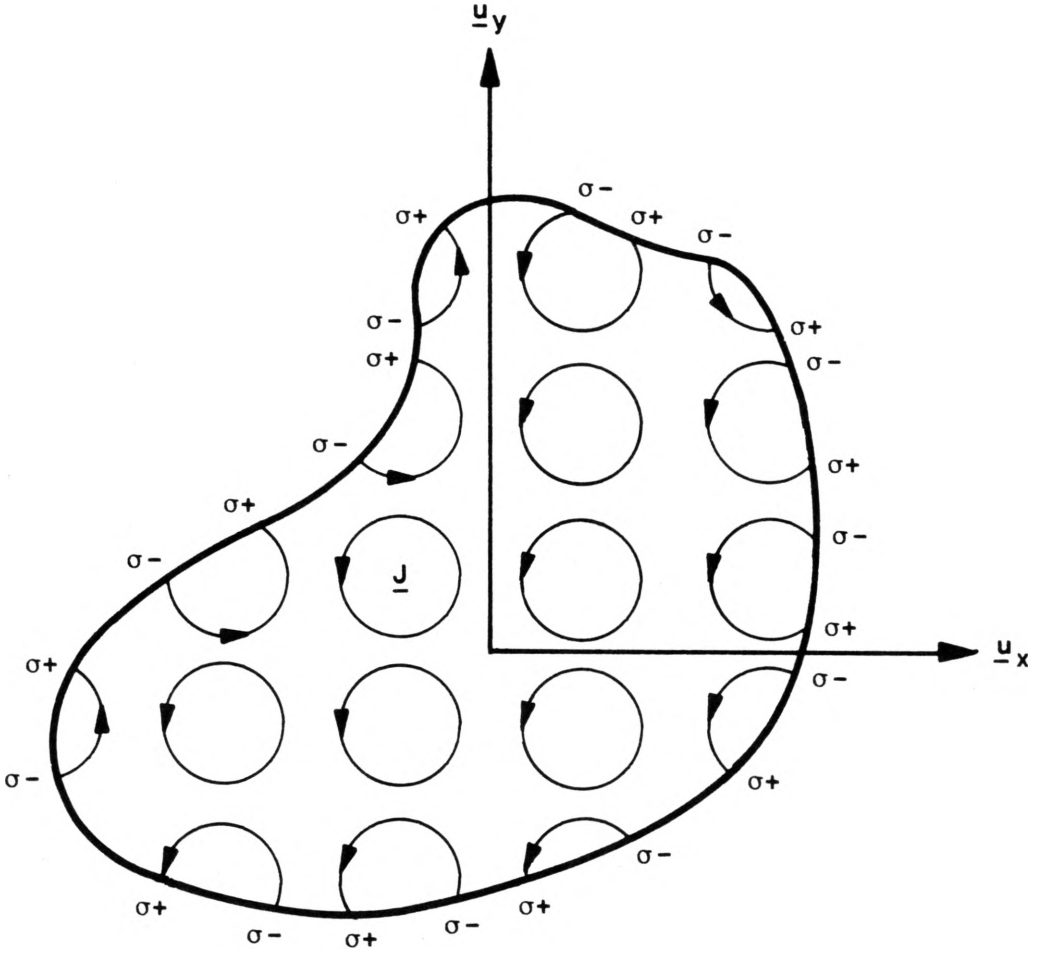

Figure 4. Circulating Current Loops and Surface Charge Doublets in a Two-Dimensional Cross-Section of a Dielectric Body

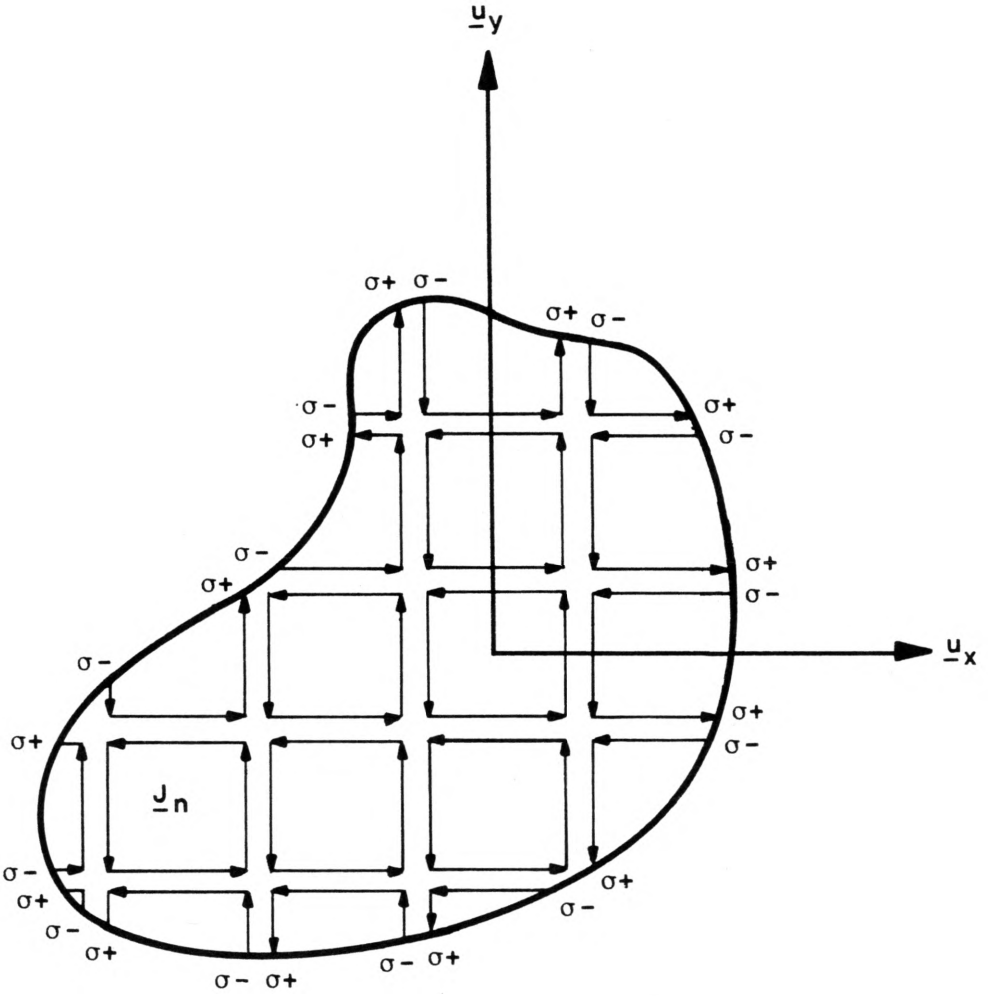

Figure 5. $\underline{u}_x$ and $\underline{u}_y$ Components of Circulating Polarization Current in a Dielectric Body with Partial Loops Terminating in Surface Charge

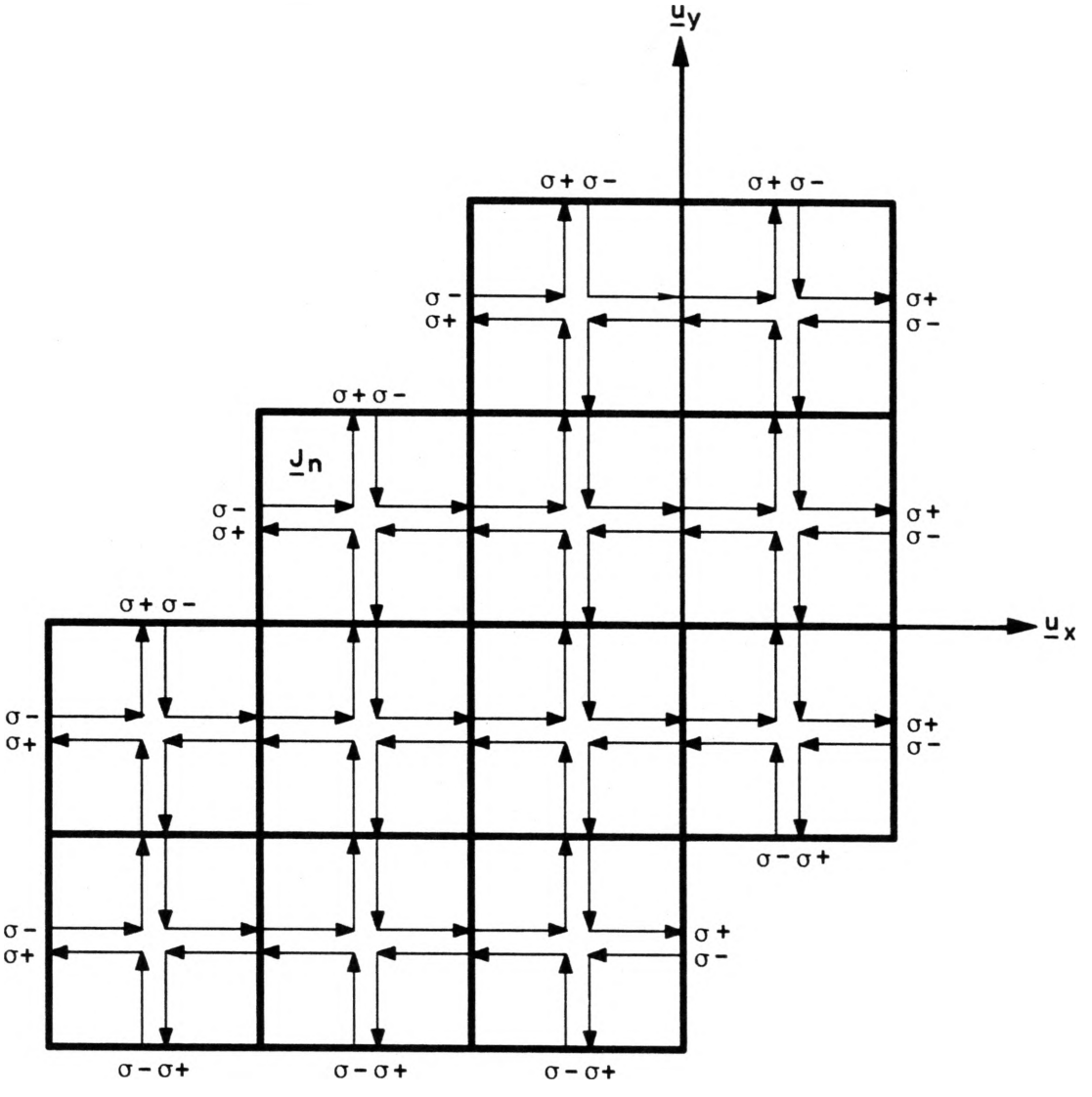

Figure 6. Twelve Cell Model of Dielectric Cross-Sectional Area and Polarization Current Loop Orientation

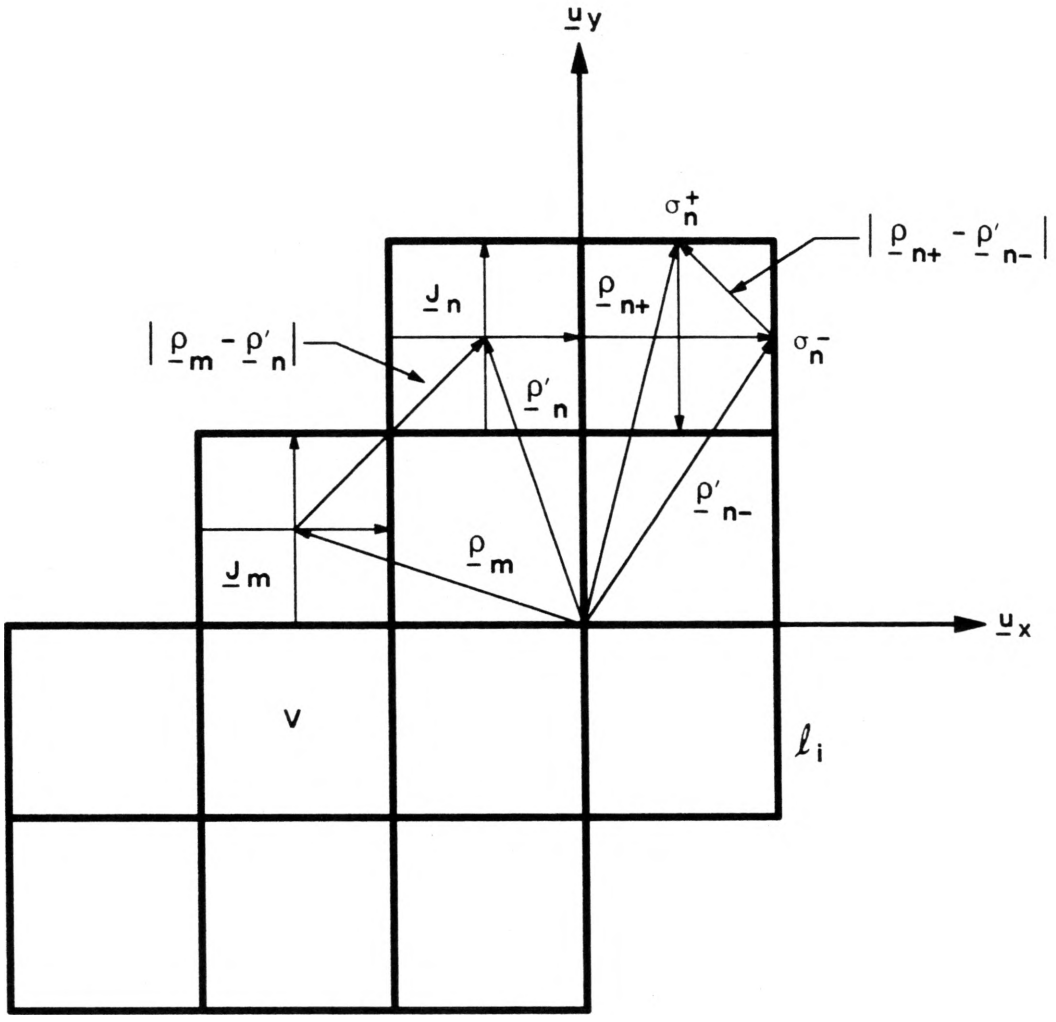

Figure 7. Local Coordinates for Polarization Current and Surface Charge Density Source and Observation Points

A rooftop function is the summation of two half rooftop functions where the right triangular functions are aligned to form an isosceles triangular base (i.e., T(x)P(y) functions having a base which lies in the xz plane, T(y)P(x) functions having a base which lies in the yz plane). The amplitudes of the rooftop functions are chosen to produce zero volume charge density and surface charge doublets at the dielectric boundary. Figure 8 shows the cross-section of a square dielectric post divided into four cells with four corner quarter current loops, four side half current loops, and one center full current loop defined over the area. The partial loops yield charge doublets where they terminate on the surface (dielectric boundary). The quarter current loop $\underline{J}_1$ defined in the first cell (N = 1) would be two half rooftop functions of magnitude equal to a triangle function of x times a pulse function of y in $-\underline{u}_x$, plus a triangle function of y times a pulse function of x in $\underline{u}_y$ shown pictorially in Figure 9. The divergence of these half rooftop functions (the volume charge density) would be a negative pulse function of x of amplitude $\frac{1}{\Delta}$ times a pulse function of y plus a pulse function of y of amplitude $\frac{1}{\Delta}$ times a pulse function of x summing to zero. This results only in a surface charge doublet (σ^+, σ^-) across the exterior sides of the cell corner in which the components of currents terminate (Figure 9).

The half current loop $\underline{J}_2$ defined across cells one and two consists of a rooftop function plus a half rooftop function in the first and second cells as shown in Figure 10. The surface charge associated with this expansion would be a pulse charge doublet (σ^+, σ^-) over the exterior left side boundary of cell one and two (Figure 10). For the full circulating current loop $\underline{J}_9$ in the center of the area, four rooftop functions are used for expansion over cells one–two, two–three, three–four, and four–one as shown in Figure 11. The rooftop expansion spanning cells four and one would be a sum of two $\underline{u}_x$ directed triangular functions of x times orthogonal pulse functions of y. The divergence of this current function would be a pulse charge doublet of x times a pulse of y, as illustrated in Figure 12. The addition of charges associated with all four rooftop functions (one–two, two–three, three–four, and four–one) cancel, yielding zero net volume charge density with a current circulating around the center of the four cell area of the dielectric cross-section.

The rooftop function satisfies the equation of continuity in the homogeneous area by proper choice of the expansion amplitudes. To obtain a set of linearly independent equations, any one loop in the cross-sectional area must be eliminated. Numerical results are given for scattering from two-dimensional models and a three-dimensional model of a cube. The results are compared to surface equivalence formulation results using a method of moments solution, which represents the most accurate solution available.

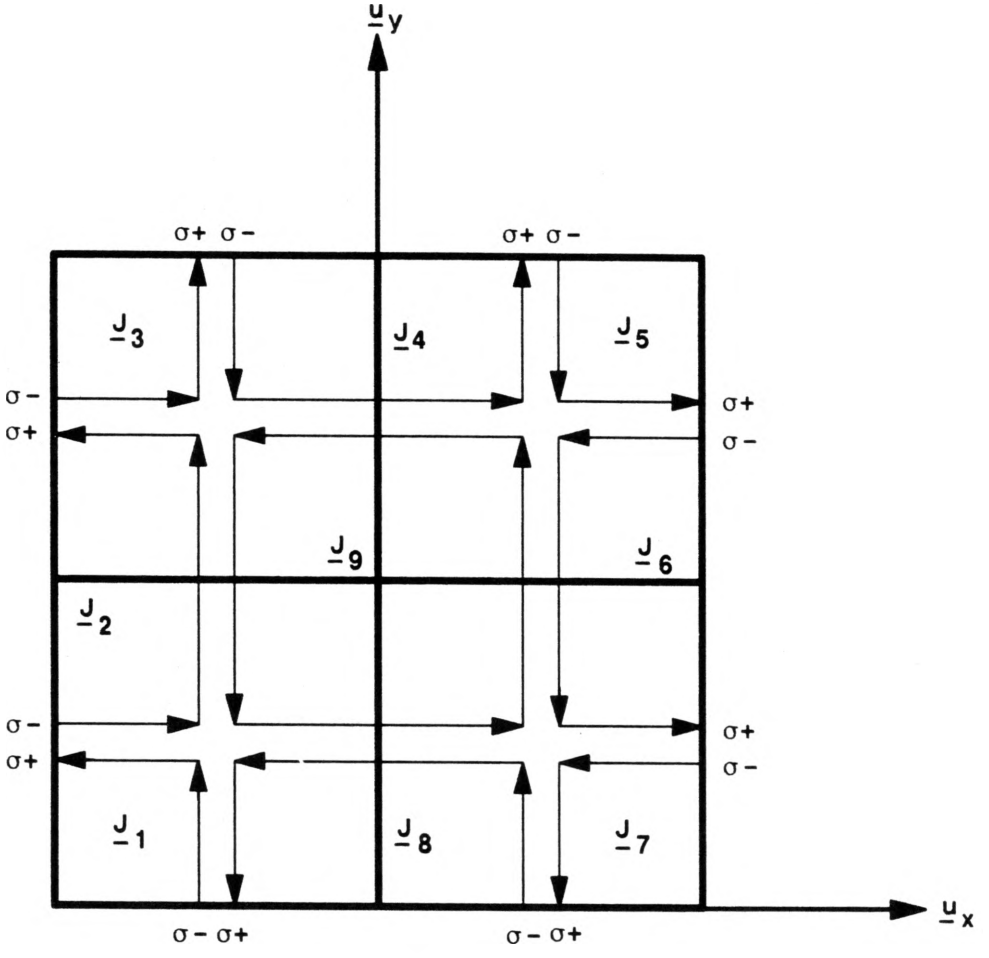

Figure 8. Four Cell Model of Dielectric Post with Polarization Current and Resulting Surface Charge Density Doublets

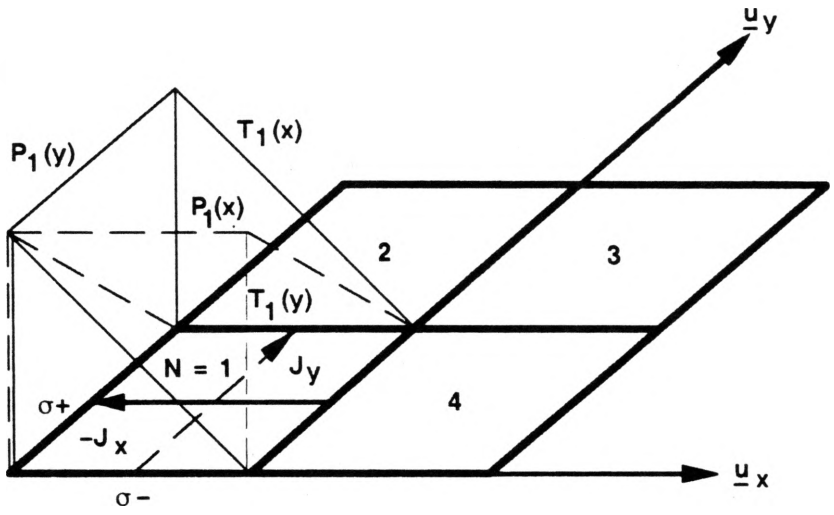

Figure 9. Quarter Current Loop and Half Rooftop Expansions Defined in First Cell and Resulting Surface Charge Doublet

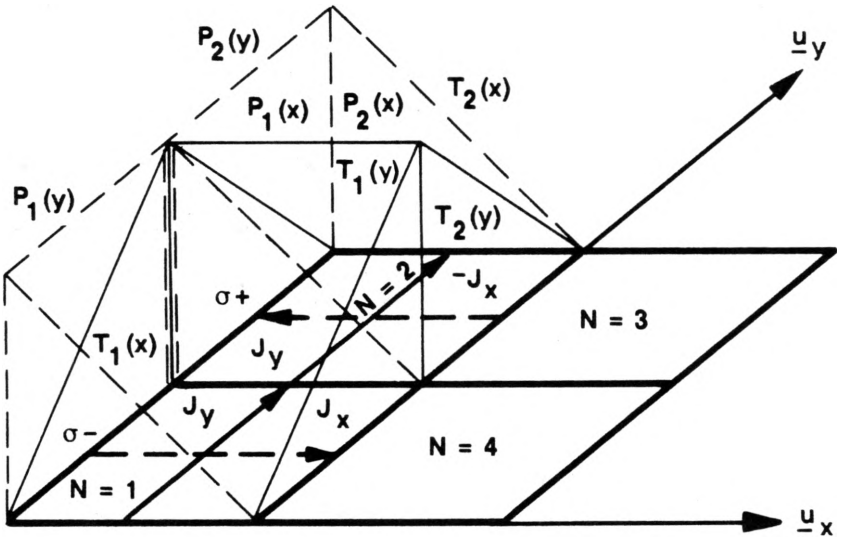

Figure 10. Half Current Loop Defined in Cells One and Two with One Rooftop and Two Half Rooftop Functions Resulting in Surface Charge Doublet

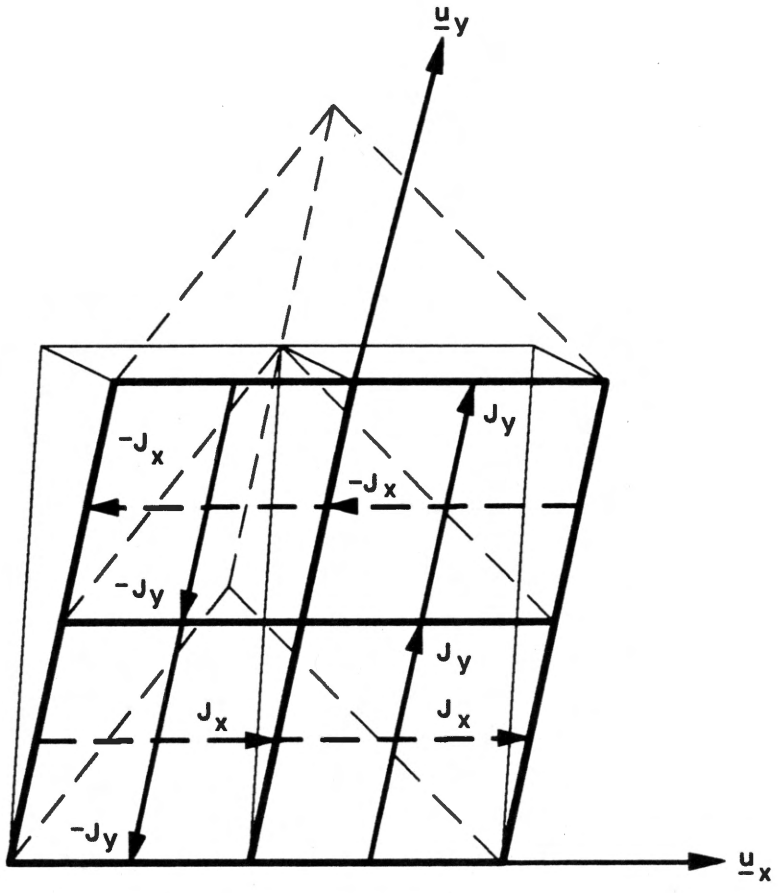

Figure 11. Full Circulating Current Loop and Associated Rooftop Expansion Functions

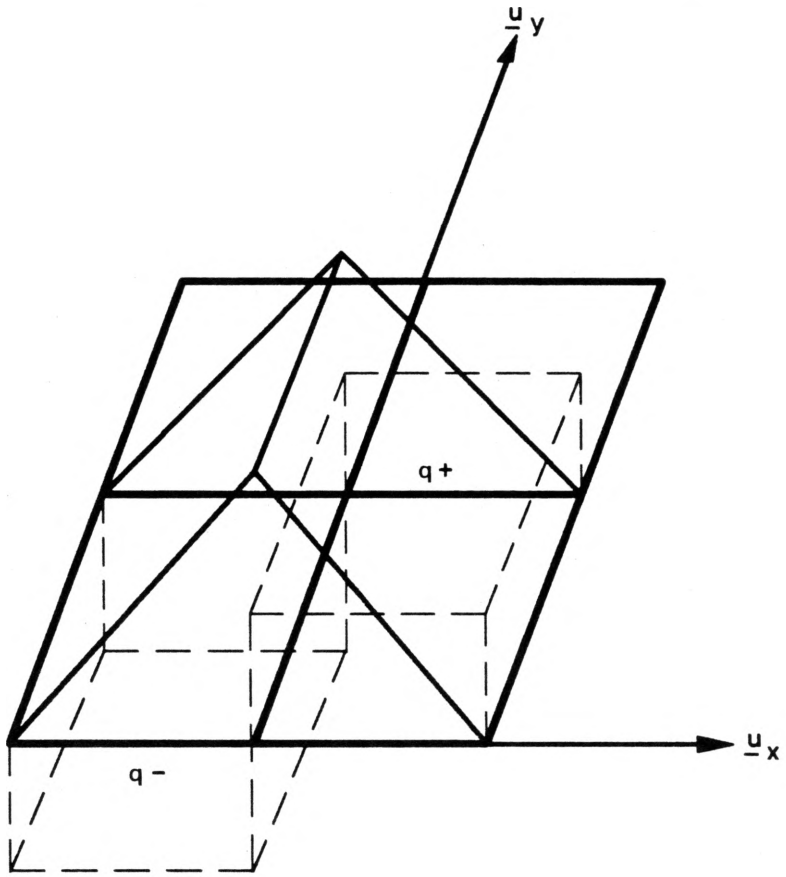

Figure 12. Divergence of J_x ($\underline{u}_x\ T_1(x)\ P_1(y) + \underline{u}_x\ T_4(x)\ P_4(y)$) Over Cells One and Four Resulting in Charge Doublet

5.0 SCATTERING FROM TWO-DIMENSIONAL HOMOGENEOUS DIELECTRIC BODIES

This section presents the evaluation of the modified impedance matrix elements and the numerical solution for TE plane wave scattering from two-dimensional homogeneous dielectric square cylinders (posts) and thin dielectric substrates (slabs). For the two-dimensional problem of scattering from a dielectric body using N square cells for modeling, the operator equation can be solved using the matrix solution developed in (3.21) and (3.25).

5.1 Evaluation of Modified Impedance Matrix Elements for a One Cell Model of Square Post

A one cell model of a two-dimensional square dielectric post is used to solve for the bistatic scattered field. The square post is shown in Figure 13 with side lengths of $\Delta X_i = \Delta Y_i$. The post is offset from the origin of the $\underline{u}_x$ axis and a uniform incident TE plane wave is incident (normal to the $\underline{u}_z$ axis) in the $\underline{k}_i$ direction at an angle ϕ_i (Figure 13). For an N cell model with no full center loops defined, there are 2(N+1) partial loops in the area. The four partial quarter current loops defined over the one cell area of the square post are depicted in Figure 14. Half rooftop functions are chosen for the $\underline{u}_x$ and $\underline{u}_y$ components of each current expansion function satisfying $\nabla \cdot \underline{J}_n = 0$ in the interior. The current $\underline{J}$ is then approximated by

$$\underline{J} = \sum_{n=1}^{2(N+1)} I_n \underline{J}_n \tag{5.1}$$

The half rooftop expansion functions $\underline{J}_n$ are defined for each partial nth loop as

$$\underline{J}_n = \begin{cases} \underline{u}_x \ell T_n(x) P_n(y) + \underline{u}_y p T_n(y) P_n(x) & \begin{cases} n=1,2,\ldots 2(N+1): \\ \ell = -1,\ n=1,\ 4 \quad p = -1,\ n=3,\ 4 \\ \ell = 1,\ n=2,\ 3 \quad p = 1,\ n=1,\ 2 \end{cases} \\ 0 & \text{otherwise} \end{cases} \tag{5.2}$$

where the half rooftop functions defined over the cell area in the $\underline{u}_x$ direction are given by

$$T_n(x) = \begin{cases} \left(-\dfrac{x}{\Delta X_i} + \dfrac{1}{2}\right) & n=1,\ 2 \quad -\dfrac{\Delta X_i}{2} \le x \le \dfrac{\Delta X_i}{2} \\ \left(\dfrac{x}{\Delta X_i} + \dfrac{1}{2}\right) & n=3,\ 4 \quad -\dfrac{\Delta X_i}{2} \le x \le \dfrac{\Delta X_i}{2} \\ 0 & \text{otherwise} \end{cases} \tag{5.3}$$

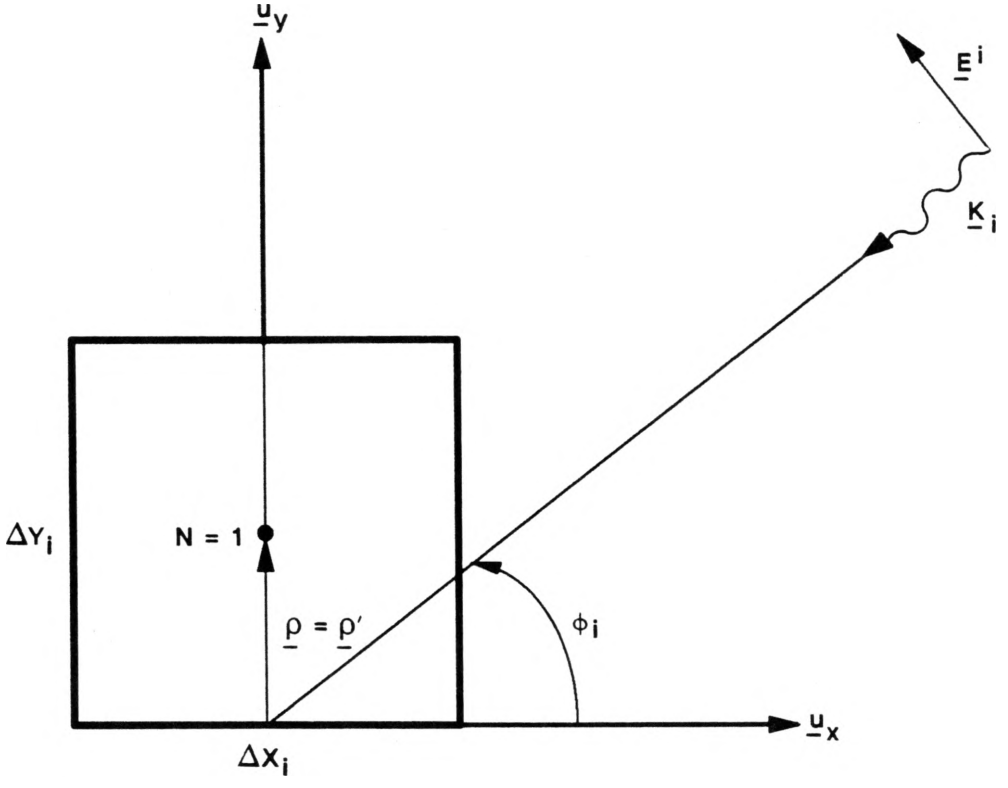

Figure 13. One Cell Model of Dielectric Post (ϵ_r = 4.0) in the Presence of a TE Plane Wave and Local Coordinates for Current Source and Field Point

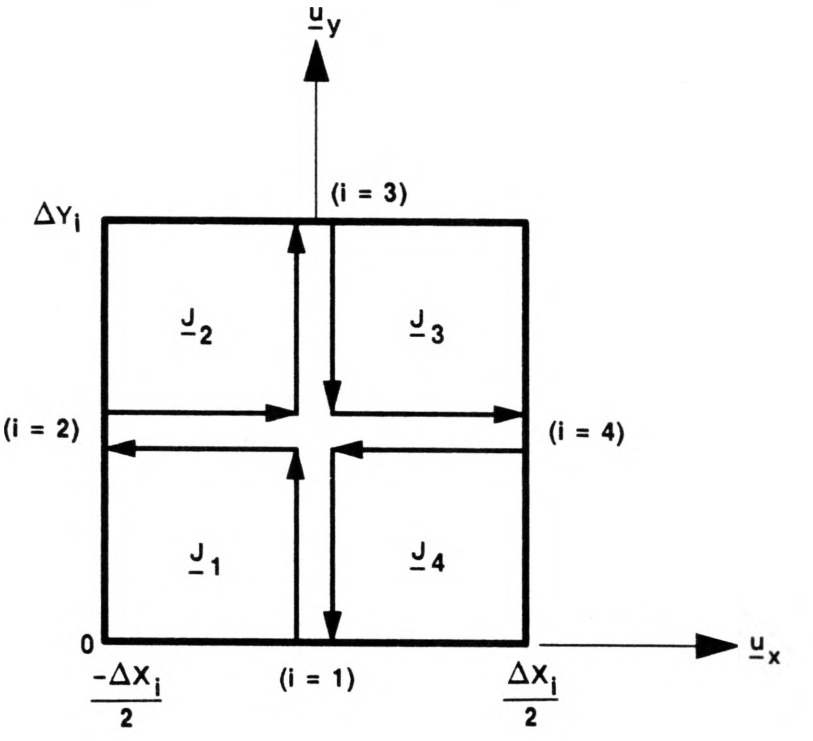

Figure 14. Four Quarter Current Loops Defined in One Cell Model of Square Dielectric Post

$$P_n(y) = \begin{cases} 1 & 0 \le y \le \Delta Y_i \\ 0 & \text{otherwise} \end{cases} \tag{5.4}$$

and in the $\underline{u}_y$ direction by

$$T_n(y) = \begin{cases} \left(1 - \frac{y}{\Delta Y_i}\right) & n=1,4 \quad 0 \le y \le \Delta Y_i \\ \left(\frac{y}{\Delta Y_i}\right) & n=2,3 \quad 0 \le y \le \Delta Y_i \\ 0 & \text{otherwise} \end{cases} \tag{5.5}$$

$$P_n(x) = \begin{cases} 1 & -\frac{\Delta X_i}{2} \le x \le \frac{\Delta X_i}{2} \\ 0 & \text{otherwise} \end{cases} \tag{5.6}$$

Figure 15 depicts the quarter loop expansion current $\underline{J}_1$ equal to a half rooftop function in the $-\underline{u}_x$ direction plus a half rooftop function in the $\underline{u}_y$ direction.

The modified impedance elements for two-dimensional problems are given by (3.25) and are determined by evaluating the vector potential terms (VP_{mn}), the scalar potential terms (SP_{mn}) and the displacement current terms (S_{mn}). For the vector potential terms, the current expansions in (5.2) are simplified by taking the average of the triangular expansions $T_n(x)$ and $T_n(y)$ as half pulse functions of the same polarization (moment) given by

$$\underline{J}_n = \begin{cases} \underline{u}_x \frac{1}{2} \ell P_n(x)\, P_n(y) + \underline{u}_y \frac{1}{2} p\, P_n(y)\, P_n(x) \begin{cases} n=1,2,\ldots 2(N+1): \\ \ell = -1,\ n=1,\ 4 \quad p = -1,\ n=3,\ 4 \\ \ell = 1,\ n=2,\ 3 \quad p = 1,\ n=1,\ 2 \end{cases} \\ 0 \qquad \text{otherwise} \end{cases} \tag{5.7}$$

This reduction of the triangular current expansions to pulse function sources simplifies evaluation of the vector potential surface integrals while maintaining the pulse doublet charge representation for the scalar potential terms.

The symmetric product integrals for the vector potential terms are further approximated by evaluating the integral at the center of the cell and multiplying by the associated area of the cell. Since the problem consists of only one cell, evaluated at the center, approximations to the integrals will all be self terms (m=n). The vector potential terms are evaluated from

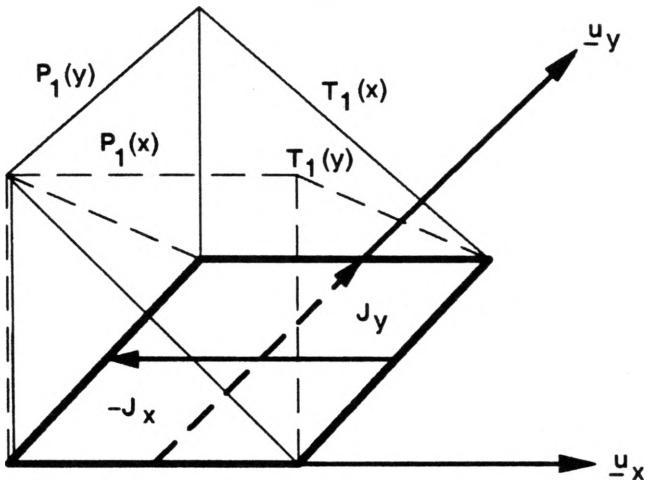

Figure 15. Half Rooftop Functions Defined in $-\underline{u}_x$ and $\underline{u}_y$ Direction for First Quarter Current Loop

$$VP_{mn} = j\omega \iint_S \underline{J}_m \cdot \underline{A}_n \, ds \tag{5.8}$$

where

$$\underline{A}_n = \frac{\mu_o}{4j} \iint_S \underline{J}_n(\underline{\rho}') \, H_o^{(2)}(k \, |\underline{\rho} - \underline{\rho}'|) \, ds' \tag{5.9}$$

Substitution of (5.9) into (5.8) gives

$$VP_{mn} = \frac{\omega\mu_o}{4} \left\{ \iint_S \underline{J}_m \cdot \left[\iint_S \underline{J}_n \, H_o^{(2)}(k \, |\underline{\rho} - \underline{\rho}'|) \, ds' \right] ds \right\} \tag{5.10}$$

$$m = 1,2, \ldots 2(N+1)$$

For self terms (m=n), the integrand is singular and a small argument formula [8] is used for the zero order Hankel functions as

$$H_o^{(2)}(k \, |\underline{\rho} - \underline{\rho}'|) \xrightarrow[|\underline{\rho} - \underline{\rho}'| \to 0]{} 1 - j \frac{2}{\pi} \log\left(\frac{\gamma k \, |\underline{\rho} - \underline{\rho}'|}{2}\right) \tag{5.11}$$

where $\gamma = 1.78107....$

The inner integral in (5.10) is evaluated by a approximating the square cell area with a circular cylinder of equal cross-sectional area as shown in Figure 16, yielding

$$\begin{aligned} A_{cell} &= A_{circle} \\ \pi \rho^2 &= \Delta X_i \Delta Y_i \\ \rho &= \sqrt{\frac{\Delta^2}{\pi}} \end{aligned} \tag{5.12}$$

where $\Delta X_i \Delta Y_i = \Delta^2$, and $\rho = a$ (the radius of the cylinder).

The transformation to polar coordinates $ds' = \rho' \, d\phi' \, d\rho'$ and substitution of the small argument formula (5.11) into the integrand of the inner integral of (5.10) results in

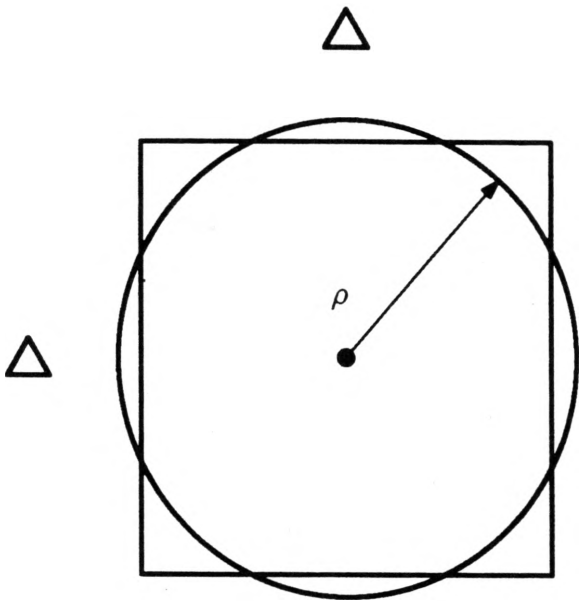

Figure 16. Cylindrical Approximation of Square Cell Area ($\rho = a$)

$$\underline{A}_n \Big|_{\rho=0} = \frac{\mu_o}{4j} \int_0^{2\pi} \int_0^{a} \underline{J}_n \left\{1 - j\frac{2}{\pi} \log\left(\frac{\gamma k \rho'}{2}\right)\right\} \rho' d\rho' d\phi'$$

$$= \frac{\mu_o \pi a^2}{4j} \left\{1 - j\frac{2}{\pi}\left[\log\left(\frac{\gamma k a}{2}\right) - \frac{1}{2}\right]\right\} \left(\frac{1}{2}\right) \left(\ell \underline{u}_x + p \underline{u}_y\right) \qquad (5.13)$$

The vector potential term is found by substitution of (5.13) into (5.8), yielding

$$VP_{mn} = \frac{\omega \mu_o \pi a^2}{8} \left\{1 - j\frac{2}{\pi}\left[\log\left(\frac{\gamma k a}{2}\right) - \frac{1}{2}\right]\right\} \int\int_S \underline{J}_m \cdot \left(\ell \underline{u}_x + p \underline{u}_y\right) ds$$

$$= \frac{\omega \mu_o \pi a^2}{8} \left\{1 - j\frac{2}{\pi}\left[\log\left(\frac{\gamma k a}{2}\right) - \frac{1}{2}\right]\right\} \int_{\frac{-\Delta X_1}{2}}^{\frac{\Delta X_1}{2}} \int_0^{\Delta Y_2} dy\, dx$$

$$= \frac{\omega \mu_o \Delta^4}{8} \left\{1 - j\frac{2}{\pi}\left[\log\left(\frac{\gamma k \sqrt{\Delta^2/\pi}}{2}\right) - \frac{1}{2}\right]\right\} \quad , m=n \qquad (5.14)$$

Integration for all other VP_{mn} terms gives

$$VP_{mn} = \begin{cases} -\frac{\mu_o \omega \Delta^4}{8} \left\{1 - j\frac{2}{\pi}\left[\log\left(\frac{\gamma k \sqrt{\Delta^2/\pi}}{2}\right) - \frac{1}{2}\right]\right\} & m+n \text{ even, } m \neq n \\ \frac{\mu_o \omega \Delta^4}{8} \left\{1 - j\frac{2}{\pi}\left[\log\left(\frac{\gamma k \sqrt{\Delta^2/\pi}}{2}\right) - \frac{1}{2}\right]\right\} & m=n \\ 0 & m+n \text{ odd} \end{cases} \qquad (5.15)$$

where n = 1, 2, ... 2(N+1) and m = 1, 2, ... 2(N+1).

The scalar potential terms SP_{mn} are evaluated from equation (3.21) as

$$SP_{mn} = \int_{\ell_i} \underline{n} \cdot \underline{J}_m \, \phi_n \, d\ell \qquad (5.16)$$

The symmetric product integrals for the scalar potential terms are approximated by evaluating the integrand at the center of the associated side segment, x_i and y_i (where i denotes the side of the cell), and multiplying by the length of the side ΔX_i or ΔY_i. The surface charge density arising from the partial current loops is shown figuratively in Figure 17, along with the local coor-

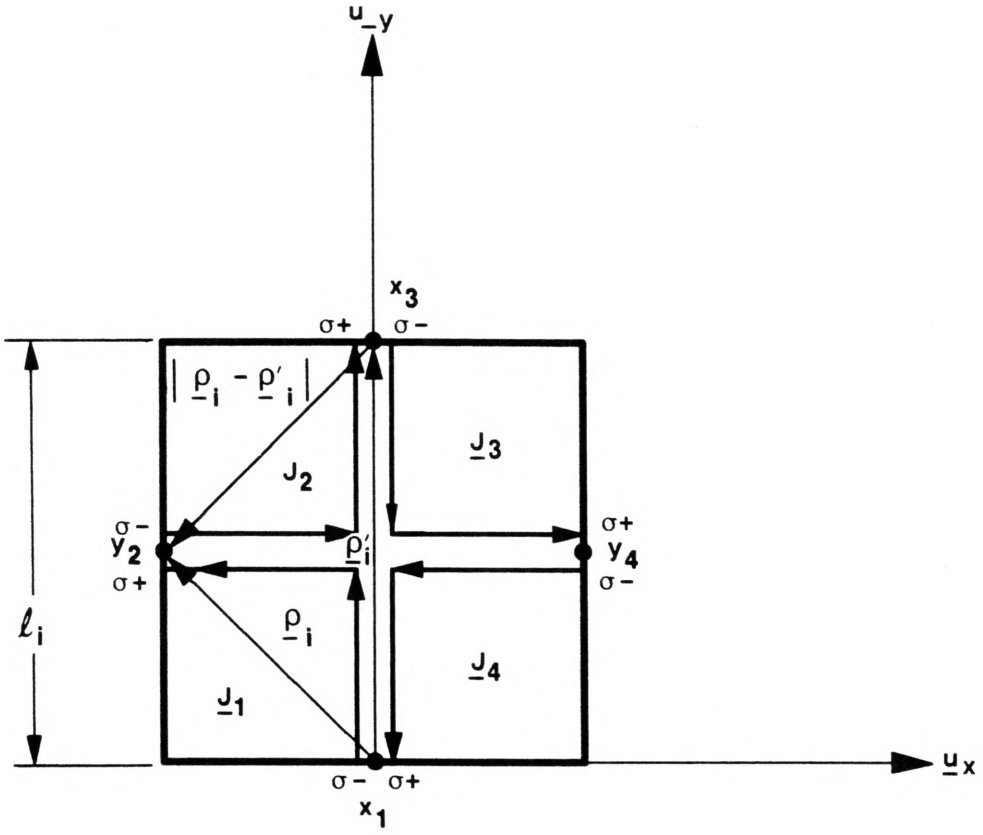

Figure 17. Local Coordinates for Surface Charge Density Doublets Source and Field Points

dinates for source and field points. Each partial current expansion $\underline{J}_n$ produces a surface charge doublet (σ^+, σ^-) on a side (i) of the cell at midpoints x_i and y_i. The current expansion functions of (5.2) give rise to surface charge according to

$$\sigma_n = \frac{1}{j\omega}\, \underline{n} \cdot \underline{J}_n \tag{5.17}$$

The surface charge doublet (σ^+, σ^-) is found by substitution of the rooftop expansion functions (5.2) into (5.17), yielding

$$\sigma_n^+ = \begin{cases} \frac{1}{j\omega}\,(1)\, P_n(x) & n=2,4 \quad x \in \Delta X_i \\ \frac{1}{j\omega}\,(1)\, P_n(y) & n=1,3 \quad y \in \Delta Y_i \\ 0 & \text{otherwise} \end{cases} \tag{5.18}$$

and

$$\sigma_n^- = \begin{cases} -\frac{1}{j\omega}\,(1)\, P_n(x) & n=1,3 \quad x \in \Delta X_i \\ -\frac{1}{j\omega}\,(1)\, P_n(y) & n=2,4 \quad y \in \Delta Y_i \\ 0 & \text{otherwise} \end{cases} \tag{5.19}$$

where (1) in (5.18) and (5.19) are the amplitudes of the triangular functions $T_n(x)$ on side i of ΔY_i and $T_n(y)$ on side i of ΔX_i.

The scalar potential terms in doublet form from (5.16) are given by

$$SP_{mn} = \frac{1}{4j\,\epsilon_o} \left\{ \int_{\ell_i} \underline{n} \cdot \underline{J}_m \left[\int_{\ell_i} \left(\sigma_n^+ + \sigma_n^- \right) H_o^{(2)} \left(k|\underline{\rho}_i - \underline{\rho}'_i| \right) d\ell' \right] d\ell \right\} \tag{5.20}$$

$$m = 1,2, \ldots 2(N+1)$$

Evaluation of ϕ_n (3.27) for the self terms (m=n) gives

$$\phi_n = \phi(\sigma_n) = -\frac{1}{4\omega\epsilon_o}\left[\int_{\ell_i} P_n(y_{n+1})\, H_o^{(2)}\left(k|\underline{\rho}_i - \underline{\rho}'_{n+1}|\right) d\ell' - \int_{\ell_i} P_n(x_n)\, H_o^{(2)}\left(k|\underline{\rho}_i - \underline{\rho}'_n|\right) d\ell'\right] \tag{5.21}$$

substitution of (5.21) into (5.16) and testing with $\underline{J}_m = \underline{J}_n$, m=n

$$\begin{aligned} SP_{mn} &= -\frac{1}{4\omega\epsilon_o}\int_{\ell_i}\left[P_n(y_{n+1}) - P_n(x_n)\right]\left\{\int_{\ell_i} P_n(y_{n+1})\, H_o^{(2)}\left(k|\underline{\rho}_i - \underline{\rho}'_{n+1}|\right) d\ell' \right. \\ &\quad \left. - \int_{\ell_i} P_n(x_n)\, H_o^{(2)}\left(k|\underline{\rho}_i - \underline{\rho}'_n|\right) d\ell'\right\} d\ell \\ &= -\frac{1}{4\omega\epsilon_o}\left\{\int_{\ell_i} P_n(y_{n+1})\left[\int_{\ell_i} P_n(y_{n+1})\, H_o^{(2)}\left(k|\underline{\rho}_{n+1} - \underline{\rho}'_{n+1}|\right) d\ell'\right] d\ell \right. \\ &\quad - \int_{\ell_i} P_n(y_{n+1})\left[\int_{\ell_i} P_n(x_n)\, H_o^{(2)}\left(k|\underline{\rho}_{n+1} - \underline{\rho}'_n|\right) d\ell'\right] d\ell \\ &\quad - \int_{\ell_i} P_n(x_n)\left[\int_{\ell_i} P_n(y_{n+1})\, H_o^{(2)}\left(k|\underline{\rho}_n - \underline{\rho}'_{n+1}|\right) d\ell'\right] d\ell \\ &\quad \left. + \int_{\ell_i} P_n(x_n)\left[\int_{\ell_i} P_n(x_n)\, H_o^{(2)}\left(k|\underline{\rho}_n - \underline{\rho}'_n|\right) d\ell'\right] d\ell\right\} \end{aligned} \tag{5.22}$$

where for n = 2(N+1), n+1 must be replaced with 1.

For improper integrals in (5.22) involving $|\underline{\rho}_n - \underline{\rho}'_n| \to 0$ and $|\underline{\rho}_{n+1} - \underline{\rho}'_{n+1}| \to 0$, the small argument approximation to the Hankel function (5.11) is used and the integration is performed over the length of the cell side. The remaining integrals are approximated by their value at the center of the respective cell side segment and multiplied by the length of the cell side. For self terms m=n, this results in

$$SP_{mn} = \frac{-\Delta^2}{2\omega\epsilon_o}\left\{-H_o^{(2)}\left(k\zeta_1\right) + \left[1 - j\frac{2}{\pi}\left(\log\left(\frac{\gamma k\Delta}{4}\right) - 1\right)\right]\right\} \tag{5.23}$$

where $\zeta_1 = |\underline{\rho}_n - \underline{\rho}'_{n+1}| = |\underline{\rho}_{n+1} - \underline{\rho}_n'| = \frac{\Delta}{\sqrt{2}}$.

Evaluation of all other SP_{mn} terms gives

$$SP_{mn} = \begin{cases} \frac{-\Delta^2}{2\omega\epsilon_o}\left\{-H_o^{(2)}\left(k\zeta_1\right) + \left[1-j\frac{2}{\pi}\left(\log\left(\frac{\gamma k\Delta}{4}\right) - 1\right)\right]\right\} & m=n \\ \frac{-\Delta^2}{4\omega\epsilon_o}\left\{-H_o^{(2)}\left(k\zeta_2\right) + 2H_o^{(2)}\left(k\zeta_1\right) - \left[1-j\frac{2}{\pi}\left(\log\left(\frac{\gamma k\Delta}{4}\right) - 1\right)\right]\right\} & |m-n|=1,3 \\ \frac{-\Delta^2}{2\omega\epsilon_o}\left\{-H_o^{(2)}\left(k\zeta_1\right) + H_o^{(2)}\left(k\zeta_2\right)\right\} & \text{otherwise} \end{cases} \quad (5.24)$$

where $\zeta_2 = |\underline{\rho}_i - \underline{\rho}'_i| = \Delta$.

The last term in equation (3.25) is the displacement current term found from (3.20). These terms are directly integrable using the rooftop expansion functions of (5.2) in

$$S_{mn} = \frac{1}{j\omega(\epsilon - \epsilon_o)} \iint_S \underline{J}_m \cdot \underline{J}_n \, ds \qquad m = 1,2, \ldots 2(N+1) \quad (5.25)$$

The self term (m=n=1) of Figure 15 describes the two half rooftop expansion functions that exist for the first quarter current loop given by

$$\underline{J}_{n=1} = -J_x + J_y \quad (5.26)$$

which is a half rooftop function in $-\underline{u}_x$ and a half rooftop function in $\underline{u}_y$ written explicitly as

$$\underline{J}_1 = -\underline{u}_x\left(\frac{-x}{\Delta X_1} + \frac{1}{2}\right)P_1(y) + \underline{u}_y\left(1 - \frac{y}{\Delta Y_2}\right)P_1(x) \quad (5.27)$$

substitution of (5.27) into (5.25) for basis and testing functions gives

$$S_{mn} = \frac{1}{j\omega(\epsilon - \epsilon_o)} \int_0^{\Delta Y_2} \int_{\frac{-\Delta X_1}{2}}^{\frac{\Delta X_1}{2}} \left\{\left[-\underline{u}_x\left(\frac{-x}{\Delta X_1} + \frac{1}{2}\right)P_1(y) + \underline{u}_y\left(1 - \frac{y}{\Delta Y_2}\right)P_1(x)\right] \cdot \left[-\underline{u}_x\left(\frac{-x}{\Delta X_1} + \frac{1}{2}\right)P_1(y) + \underline{u}_y\left(1 - \frac{y}{\Delta Y_2}\right)P_1(x)\right]\right\} dx\, dy \quad (5.28)$$

Evaluation of this dot product and integration yields

$$S_{mn} = \frac{-2j\Delta^2}{3\omega\,\epsilon_o\,(\epsilon_r - 1)} \qquad ,m = n = 1 \tag{5.29}$$

Solution for all other S_{mn} terms results in

$$S_{mn} = \begin{cases} \dfrac{-2j\Delta^2}{3\omega\,\epsilon_o\,(\epsilon_r - 1)} & m = n \\ \dfrac{j\Delta^2}{6\omega\,\epsilon_o\,(\epsilon_r - 1)} & m + n \quad \text{odd} \\ \dfrac{j\Delta^2}{3\omega\,\epsilon_o\,(\epsilon_r - 1)} & \text{otherwise} \end{cases} \tag{5.30}$$

The modified impedance matrix can be obtained from (3.21) by the summation of matrix elements (5.15), (5.24), and (5.30). To obtain a linearly independent set of modified impedance equations $\hat{Z}_{mn}$, one current expansion function $\underline{J}_n$ and the corresponding testing function $\underline{J}_m$ must be eliminated. This reduces the 2(N+1) x 2(N+1) matrix to the order of 2N+1.

5.2 Discussion of Numerical Results for a One Cell Model

The bistatic scattering cross section can be obtained using the modified impedance matrix $\hat{Z}_{mn}$ and equation (A.19). From reciprocity, the bistatic scattering cross section is given by

$$\sigma_B = \frac{\mu_o^2 \omega^2}{4k} \left| \left[\tilde{V}_m^r\right] \left[\hat{Z}_{mn}^{-1}\right] \left[V_m^i\right] \right|^2 \tag{5.31}$$

This expression is derived in Appendix A for two-dimensional scattering. In the one cell model with four quarter current loops, the last loop was neglected to obtain a linearly independent set of equations. Figure 18 shows the bistatic cross section (σ_B/λ) of a tenth wavelength square dielectric ($\epsilon_r = 4.0$) post. The uniform incident electric field is at ϕ_i equal to 90 degrees. The computed results are plotted in Figure 18, along with a surface equivalence formulation (SEF) solution which used 40 subsections (ten per side). The bistatic scattering cross section obtained from the volume integral formulation (VIF) differs from that obtained from the SEF by 5 percent in the backscattered direction ($\phi_r = 90°$) and by 19 percent in the forward scattered direction ($\phi_r = 270°$). The same VIF solution is compared to a SEF solution with four unknowns, one subsection

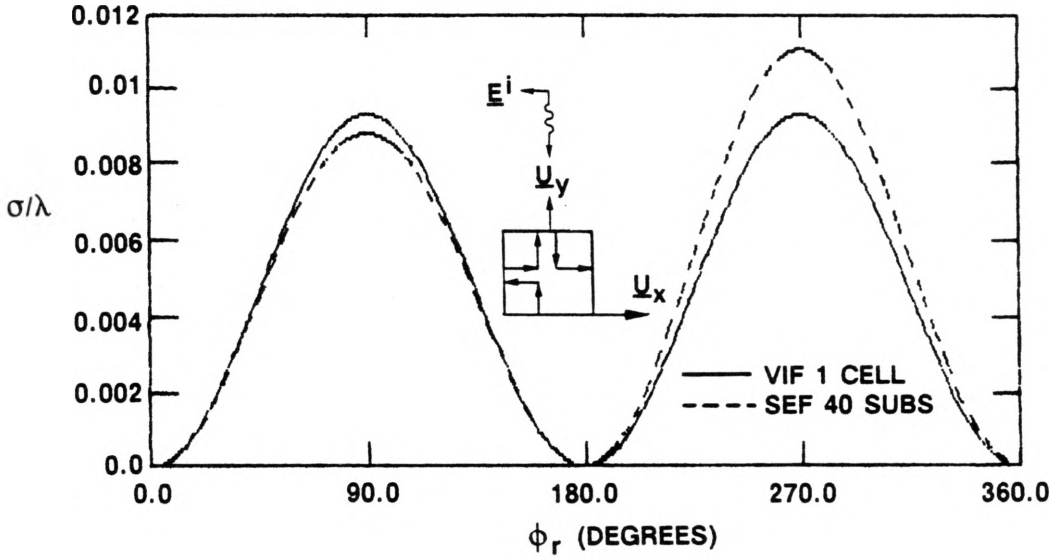

Figure 18. Bistatic Scattering (1 Cell VIF Compared with 40 Subsection SEF) from 0.1λ x 0.1λ Dielectric (ϵ_r = 4.0) Square Post, ϕ_i = 90°

per side in Figure 19 . The one cell VIF solution gives closer agreement with the 40 subsection SEF solution than the four subsection SEF result. Compared to the 40 subsection SEF results for backscattering, the four subsection SEF solution is off by 28 percent while the VIF solution is within five percent. The VIF solution shows no difference in the forward and backscattered cross section due to the single cell current expansions used. The VIF solution, which used an accurate representation of the surface charge density, gives reasonably good agreement with the SEF while using considerably fewer unknowns. The order of accuracy (forward and backscattered directions) in the VIF solution can be increased by using four cells to model the square post cross–sectional area. This results in four quarter current loops and four half current loops along with one full center current loop defined in the area.

5.3 Evaluation of Modified Impedance Matrix Elements for a Four Cell Model of Square Post

The square post area of side length Δ by Δ in Figure 13 is broken up into four cells (N=4) with 2N+1 current loops (both partial and full) defined in the area with their associated charge doublets (as shown in Figure 8). Each cell is a square whose side length is $\frac{\Delta}{2}$. The rooftop expansions used in this model are described in Section 4.2. The full center circulating current loop has neither a volume nor a surface charge density resulting from it. The vector potential terms from evaluation of (5.8) are

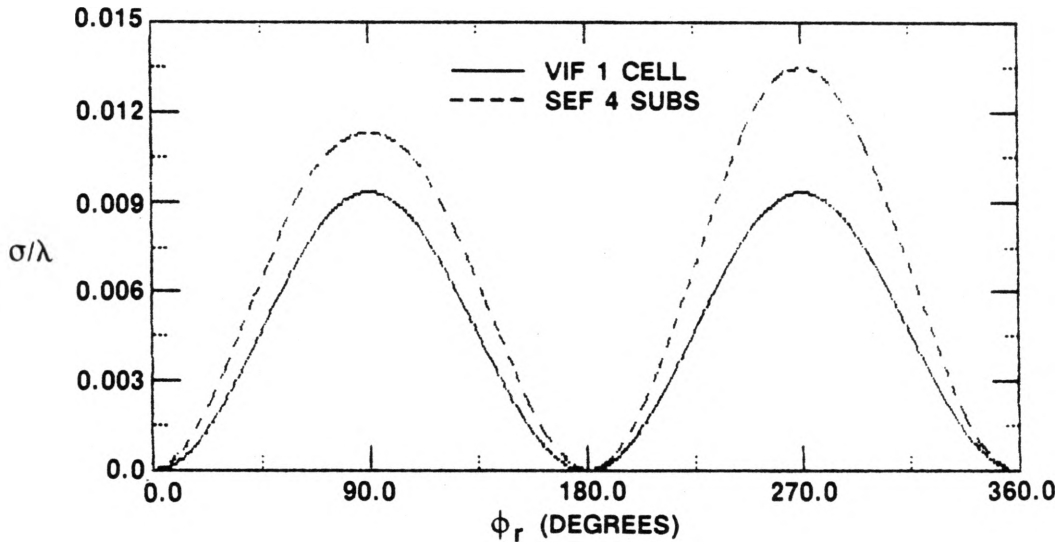

Figure 19. Bistatic Scattering (1 Cell VIF Compared with 4 Subsection SEF) from 0.1λ x 0.1λ Dielectric (ϵ_r = 4.0) Square Post, ϕ_i = 90°

$$VP_{mn} = \begin{cases} \frac{\omega\mu_o \Delta^4}{128}\left\{1 - j\frac{2}{\pi}\left[\log\left(\frac{\gamma k\sqrt{\Delta^2/4\pi}}{2}\right) - \frac{1}{2}\right]\right\} & \\ \qquad\qquad m,n \text{ odd } m = n,\ m \text{ and } n \neq 2N+1 & \\ \frac{\omega\mu_o \Delta^4}{128}\left[H_o^{(2)}\left(k\zeta_1\right)\right] \qquad |m-n| = 1,7,\ m \text{ and } n \neq 2N+1 & \\ 0 \qquad \begin{cases} |m-n| = 2,6 \ m,n \text{ odd},\ m \text{ and } n \neq 2N+1 \\ |m-n| = 1,3,5,7,\ m \text{ or } n = 2N+1 \end{cases} & \\ -\frac{\omega\mu_o \Delta^4}{128}\left[H_o^{(2)}\left(k\zeta_1\right)\right] \qquad |m-n| = 3,5 \text{ and } n \neq 2N+1 & \\ -\frac{\omega\mu_o \Delta^4}{128}\left[H_o^{(2)}\left(k\zeta_2\right)\right] \quad |m-n| = 4 \ m,n \text{ odd},\ m \text{ and } n \neq 2N+1 & \\ \frac{\omega\mu_o \Delta^4}{128}\left\{-\left[1 - j\frac{2}{\pi}\left(\log\left(\frac{\gamma k\sqrt{\Delta^2/4\pi}}{2}\right) - \frac{1}{2}\right)\right]\right. & \\ \qquad \left. + H_o^{(2)}\left(k\zeta_2\right)\right\} \quad \begin{cases} |m-n| = 2,6 \text{ and } m,n \text{ even} \\ |m-n| = 2,4,6,8, \text{ and } m \text{ or } n = 2N+1 \end{cases} & \\ \frac{\omega\mu_o \Delta^4}{64}\left\{1 - j\frac{2}{\pi}\left(\log\left(\frac{\gamma k\sqrt{\Delta^2/4\pi}}{2}\right) - \frac{1}{2}\right)\right\} \qquad m = n \quad m,n \text{ even} & \\ -\frac{\omega\mu_o \Delta^4}{64}\left[H_o^{(2)}\left(k\zeta_2\right)\right] \qquad |m-n| = 4 \ m,n \text{ even} & \\ \frac{\omega\mu_o \Delta^4}{32}\left\{\left[1 - j\frac{2}{\pi}\left(\log\left(\frac{\gamma k\sqrt{\Delta^2/4\pi}}{2}\right) - \frac{1}{2}\right)\right]\right. & \\ \qquad \left. - H_o^{(2)}\left(k\zeta_2\right)\right\} \qquad m,n = 2N+1 & \end{cases} \tag{5.32}$$

where the distances from observation point to source point at the center of the cells are given in Figure 20 as ζ_i ($\zeta_1 = \frac{\Delta}{2}$, $\zeta_2 = \frac{\Delta}{\sqrt{2}}$) for all VP_{mn} terms.

The scalar potential terms evaluated from (5.16) are

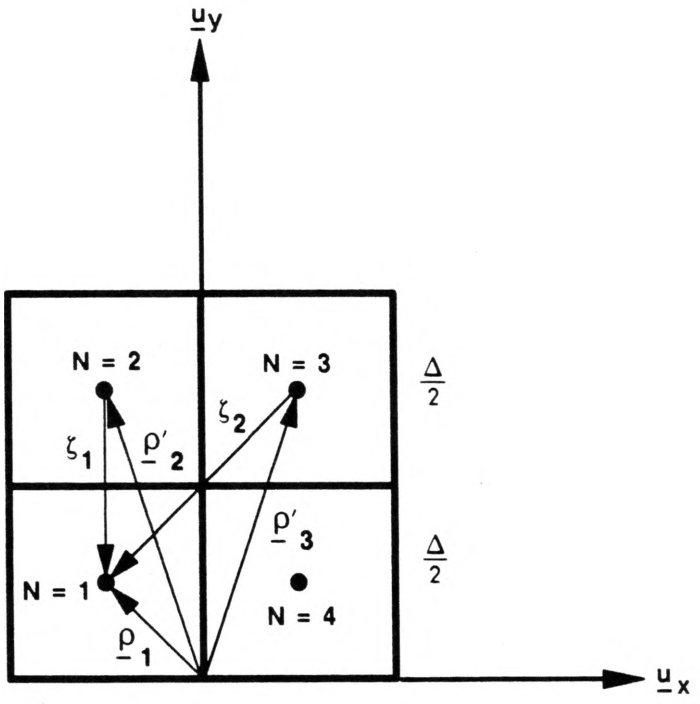

Figure 20. Point Matching Locations for Polarization Current Coordinates for Source and Observation Distances in Four Cell Model

$$SP_{mn} = \begin{cases} -\frac{\Delta^2}{8\omega\epsilon_o}\left[\left(1 - j\frac{2}{\pi}\left(\log\left(\frac{\gamma k\Delta}{8}\right) - 1\right)\right) - H_o^{(2)}\left(k\beta_\ell\right)\right] & \begin{cases} m = n \\ \ell = 1 \text{ for m odd} \\ \ell = 2 \text{ for m even} \end{cases} \\ -\frac{\Delta^2}{16\omega\epsilon_o}\left[-\left(1 - j\frac{2}{\pi}\left(\log\left(\frac{\gamma k\Delta}{8}\right) - 1\right)\right) + H_o^{(2)}\left(k\beta_1\right) + H_o^{(2)}\left(k\beta_2\right) - H_o^{(2)}\left(k\beta_3\right)\right] & |m-n| = 1,7 \\ -\frac{\Delta^2}{16\omega\epsilon_o}\left[-H_o^{(2)}\left(k\beta_6\right) + 2\,H_o^{(2)}\left(k\beta_3\right) - H_o^{(2)}\left(k\beta_2\right)\right] & m,n \text{ odd } |m-n| = 2,6 \\ -\frac{\Delta^2}{16\omega\epsilon_o}\left[2\,H_o^{(2)}\left(k\beta_3\right) - H_o^{(2)}\left(k\beta_4\right) - H_o^{(2)}\left(k\beta_1\right)\right] & m,n \text{ even } |m-n| = 2,6 \\ -\frac{\Delta^2}{8\omega\epsilon_o}\left[H_o^{(2)}\left(k\beta_5\right) - H_o^{(2)}\left(k\beta_4\right)\right] & m,n \text{ odd } |m-n| = 4 \\ -\frac{\Delta^2}{8\omega\epsilon_o}\left[H_o^{(2)}\left(k\beta_5\right) - H_o^{(2)}\left(k\beta_6\right)\right] & m,n \text{ even } |m-n| = 4 \\ -\frac{\Delta^2}{16\omega\epsilon_o}\left[-H_o^{(2)}\left(k\beta_5\right) + H_o^{(2)}\left(k\beta_6\right) + H_o^{(2)}\left(k\beta_4\right) - H_o^{(2)}\left(k\beta_3\right)\right] & |m-n| = 3,5 \\ 0 & m \text{ or } n = 2N+1 \end{cases} \tag{5.33}$$

where the radius vectors from observation to source points are given in Figure 21 in terms of length β_j. The last entry on the right-hand side of (5.33) gives 0 for m or n = 2N+1. All other entries on the right-hand side of (5.33) are for $m \neq 2N+1$ and $n \neq 2N+1$.

Evaluation of the displacement current terms from (5.25) gives

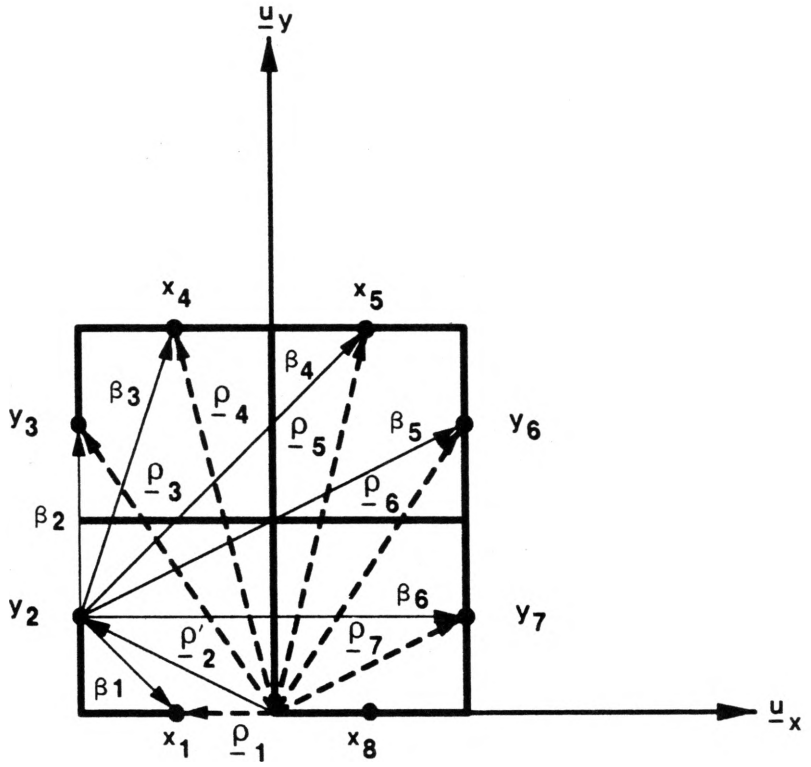

Figure 21. Local Coordinates for Point Matching Locations for Surface Charge Density Source and Observation Points for Scalar Potential Terms in Four Cell Model

$$
S_{mn} = \begin{cases}
\dfrac{-j\Delta^2}{6\omega\,\epsilon_o\,(\epsilon_r - 1)} & m = n \quad m,n \text{ odd} \quad m \text{ and } n \neq 2N+1 \\
\dfrac{-j\Delta^2}{3\omega\,\epsilon_o\,(\epsilon_r - 1)} & m = n \quad m,n \text{ even} \\
\dfrac{-2j\Delta^2}{3\omega\,\epsilon_o\,(\epsilon_r - 1)} & m,n = 2N+1 \\
\dfrac{j\Delta^2}{24\omega\,\epsilon_o\,(\epsilon_r - 1)} & |m-n| = 1,7 \quad m \text{ and } n \neq 2N+1 \\
0 & \begin{cases} |m-n| = 3,4,5 & m \text{ and } n \neq 2N+1 \\ |m-n| = 2,6 & m,n \text{ odd} \quad m \text{ and } n \neq 2N+1 \end{cases} \\
\dfrac{j\Delta^2}{12\omega\,\epsilon_o\,(\epsilon_r - 1)} & \begin{cases} |m-n| = 2 & m,n \text{ even} \quad m \text{ and } n \neq 2N+1 \\ |m-n| = 2 & m,n \text{ odd} \quad m \text{ or } n = 2N+1 \\ |m-n| = 6 & m,n \text{ even} \quad m \text{ and } n \neq 2N+1 \\ |m-n| = 6 & m,n \text{ odd} \quad m \text{ or } n = 2N+1 \\ |m-n| = 1,3,4,5,7,8 & m \text{ or } n = 2N+1 \end{cases}
\end{cases} \tag{5.34}
$$

Leaving out the last partial loop reduces the 2N+1 matrix to the order of 2N.

5.4 Discussion of Numerical Results of the Four Cell Model

The bistatic scattering (ϕ_i=90°) is shown in Figure 22 for the four cell VIF, with the last partial current loop removed, compared to the 40 subsection SEF solution. The VIF solution gives excellent agreement (within one percent) in the backscattered direction (ϕ_r=90°) with the SEF solution. The forward scattered pattern at ϕ_r=270° differs with the SEF result by 4.5 percent. This agreement is noteworthy, considering the small number of unknowns taken in the VIF solution. Comparisons were made between the VIF results and a four and an eight subsection SEF solution. These comparisons are shown in Figures 23 and 24, respectively. From these plots, the eight subsection (two subsections per side) SEF solution only approaches the 40 subsection SEF within a nine percent margin. Figure 25 shows an overlay of all five solutions, showing dramatically the rate at which the VIF solution approaches the best solution relative to the SEF results using a comparably few number of unknowns.

5.5 Discussion of Numerical Results for a thin Dielectric Slab

The bistatic scattering from a two-dimensional dielectric slab was obtained and compared to a SEF and a finite element solution. The results were also compared to previously published results of Richmond [4]. Figure 26 shows a dielectric slab of N cells with 2(N+1) partial current loops. A general purpose program was written to subdivide the N cell slab (N>5), compute the modified

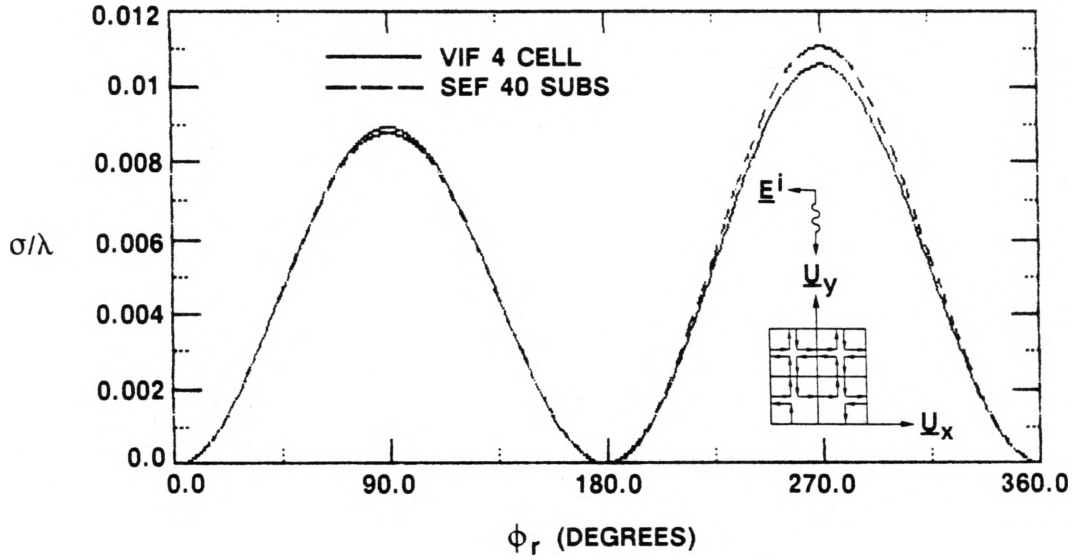

Figure 22. Bistatic Scattering (4 Cell VIF Compared with 40 Subsection SEF) from 0.1λ x 0.1λ Dielectric (ϵ_r = 4.0) Square Post, ϕ_i = 90°

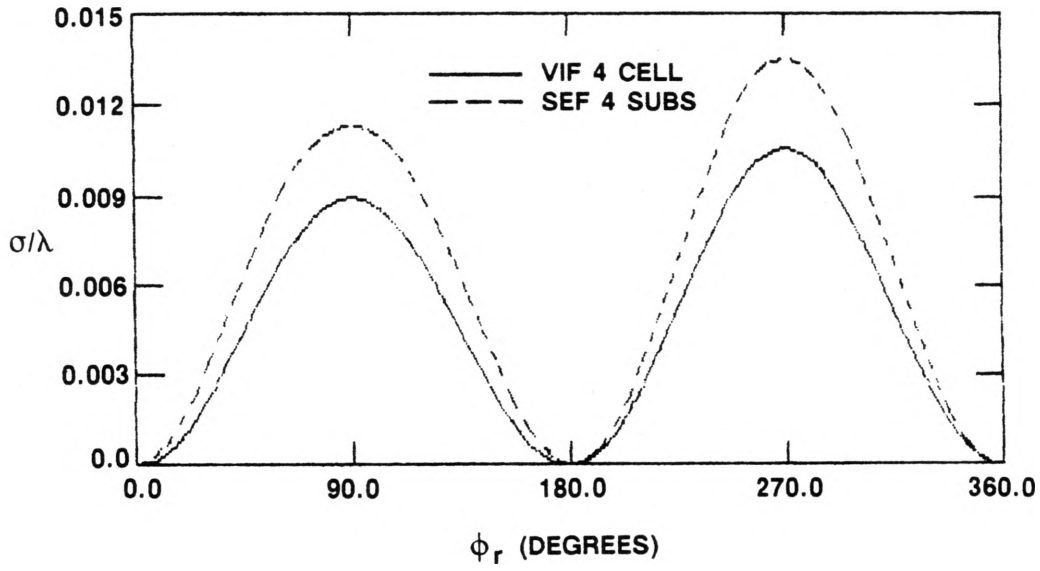

Figure 23. Bistatic Scattering (4 Cell VIF Compared with 4 Subsection SEF) from 0.1λ x 0.1λ Dielectric (ϵ_r = 4.0) Square Post, ϕ_i = 90°

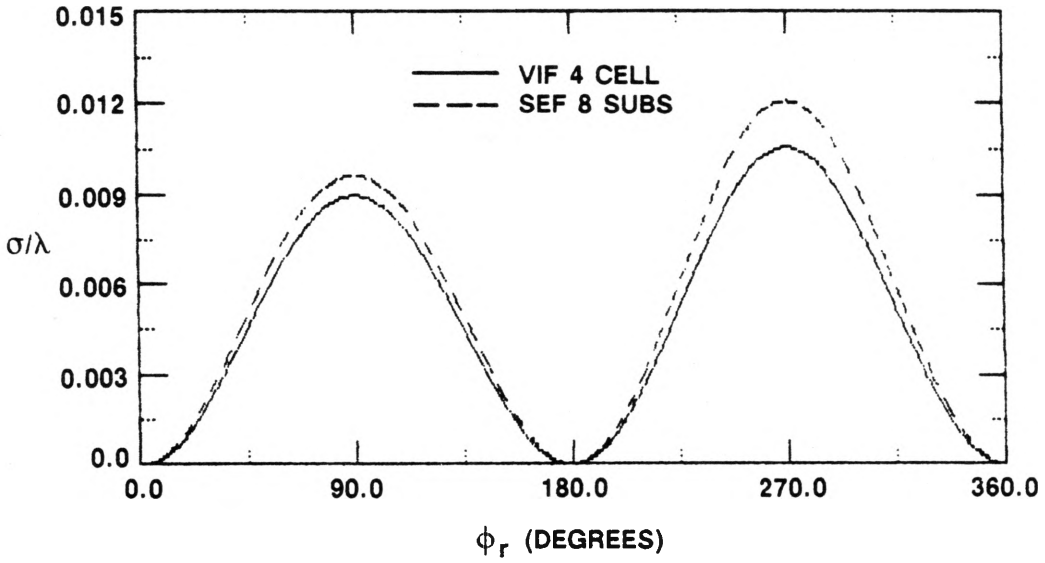

Figure 24. Bistatic Scattering (4 Cell VIF Compared with 8 Subsection SEF) from 0.1λ x 0.1λ Dielectric (ϵ_r = 4.0) Square Post, ϕ_i = 90°

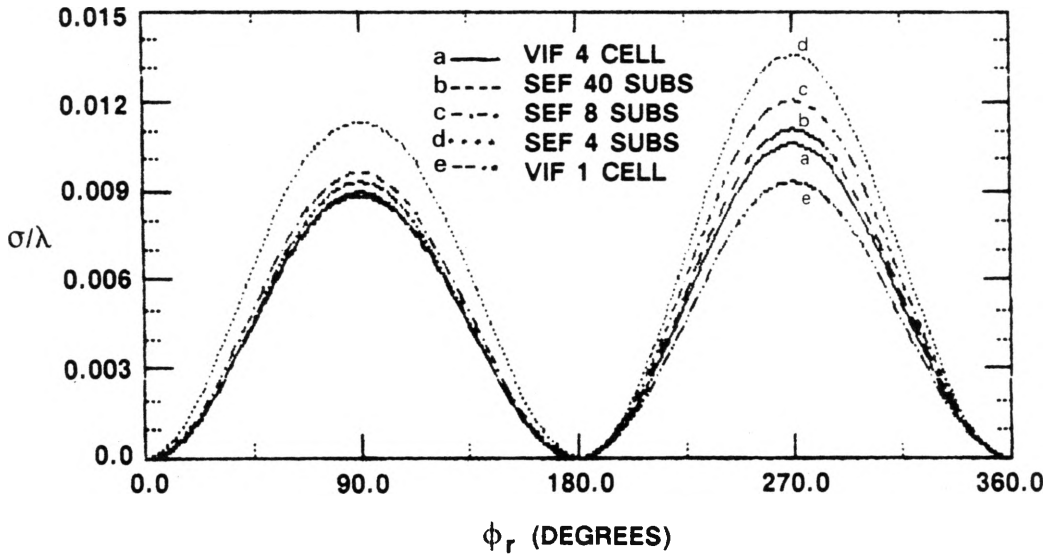

Figure 25. One and Four Cell VIF Comparison to Four, Eight and 40 Subsection SEF Bistatic Scatterings Solutions from 0.1λ x 0.1λ Dielectric (ϵ_r = 4.0) Square Post, ϕ_i = 90°

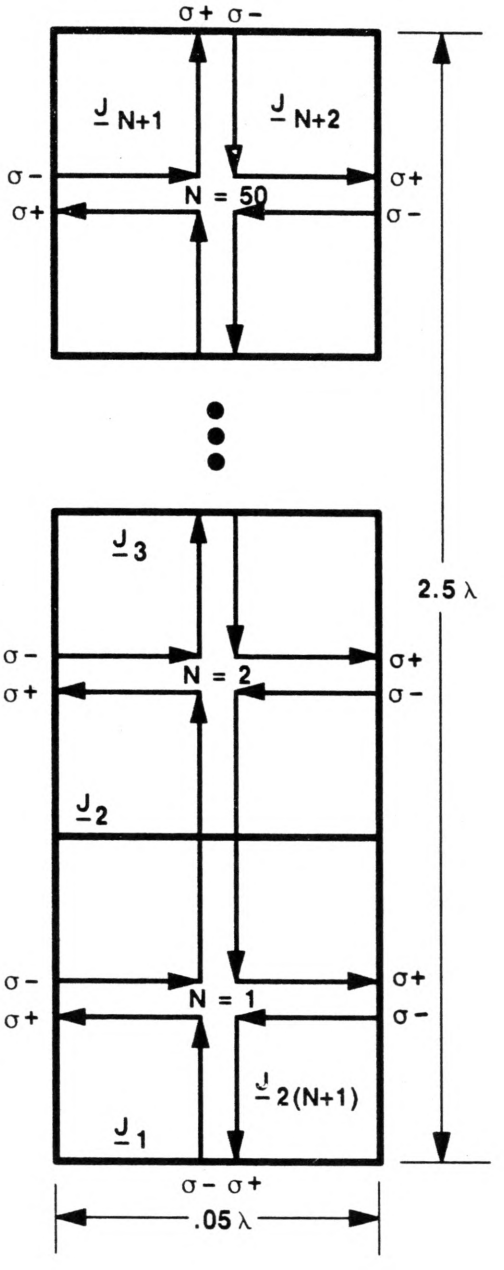

Figure 26. 50 Cell Model of Dielectric Slab ($\epsilon_r = 4.0$) and Partial Circulating Current Loops

impedance matrix elements, and to solve for the bistatic scattered field. An exemplary case of a dielectric slab having a relative permittivity of 4.0 and a length of 2.5λ and a 0.05λ thickness was modeled using 50 cells. The scattered field was computed using the VIF as was developed earlier in this section using a one cell model. A bistatic scattering pattern from a normally incident (ϕ_i=180°) wave is shown in Figure 27, comparing a 50 cell VIF solution with a 210 subsection SEF result. Agreement in the backscattered region is excellent. A plot of the scattered field between ϕ_r equal zero and 35 degrees is presented in Figure 28. Comparisons are made between a SEF solution, a finite element (FEM) solution with 70 unknowns, Richmond's results with 50 subsectional areas, and a physical optics solution. The VIF and the physical optics solutions agree within a percent. The VIF is three percent off from the finite element solution and five percent off from the SEF at ϕ_r equal zero degrees. The agreement between all solutions is quite good out past ϕ_r equal to 25 degrees. Figure 29 is a plot of the VIF bistatic scattering at grazing incidence (ϕ_i=270°) compared to the SEF solution using 210 subsections. The solution is off by three percent in the forward scattered field due to the one cell approximation in width used in the VIF as compared to the five subsections used to model the width in the SEF solution. The VIF solution is also compared to Richmond's result and a finite element solution from ϕ_r equal 20 to 90 degrees in Figure 30. The VIF solution is within two percent of the finite element result and three percent of Richmond's results.

To observe the relative difference between the VIF and SEF solutions, a comparison was made with a SEF using 50 subsections per side and one per width. This comparison is shown in Figures 31 through Figure 34 for normal and grazing incident fields. Figure 31 shows the bistatic scattering comparison for normal incidence of the 50 cell VIF and 102 subsection SEF solution. The VIF backscattered solution differs from the SEF result by 1.1 percent as compared to a 1.4 percent difference from the more exact 210 subsection SEF result. A closer view of the bistatic scattering (ϕ_i=180°) is shown in Figure 32 with ϕ_r varying from 0 to 35 degrees. The forward scattered field is within 4.8 percent of the 102 subsection SEF results. These results show closer correlation between the 50 cell VIF and the SEF solution using 102 subsections.

The grazing incidence (ϕ_i=270°) comparison between the comparable VIF and SEF solutions is shown in Figure 33. The solution is plotted in Figure 34 with ϕ_r varying from 20 to 90 degrees. The forward scattered field differs by 3.7 percent, resulting in a larger difference between the two solutions than in the previous grazing incidence case.

The numerical solutions of the VIF compared to the SEF are extremely promising, taking into account the differences in the number of unknowns used in each case. The 50 cell VIF results were closer to the 102 subsection SEF result in the normal incident case than the 210 subsection SEF solution. The absence of a full center current loop resulted in no variation in forward and backscattered field in the VIF solution. A better approximation can be obtained with the VIF by using two cells per slab width, resulting in some full circulating current loops, as was done in the square post example to obtain a more exact solution in the forward and backscattered directions.

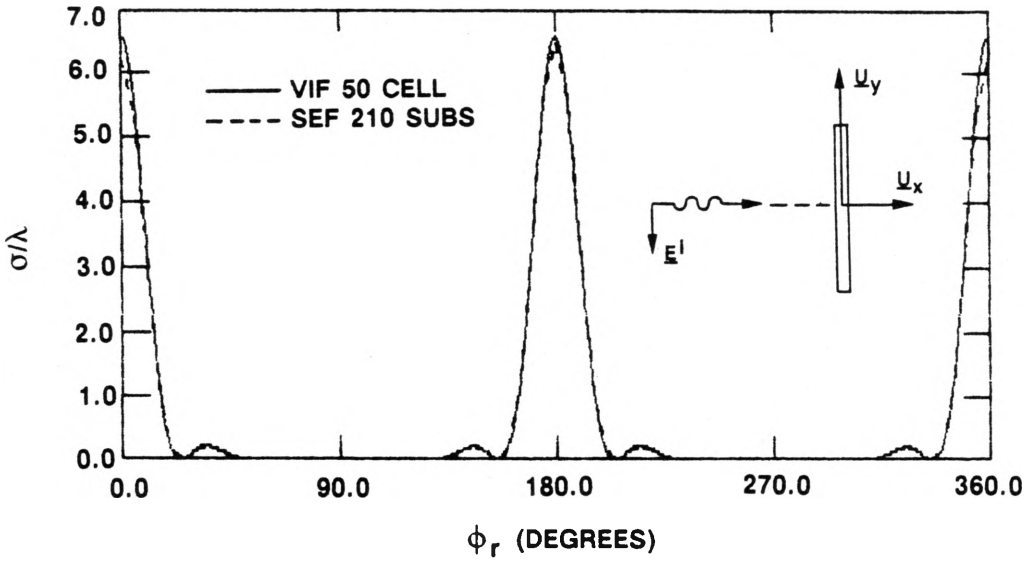

Figure 27. Bistatic Scattering, 50 Cell VIF Compared with 210 Subsection SEF, from 0.05λ x 2.5λ Dielectric (ϵ_r = 4.0) Slab. ϕ_i = 180°

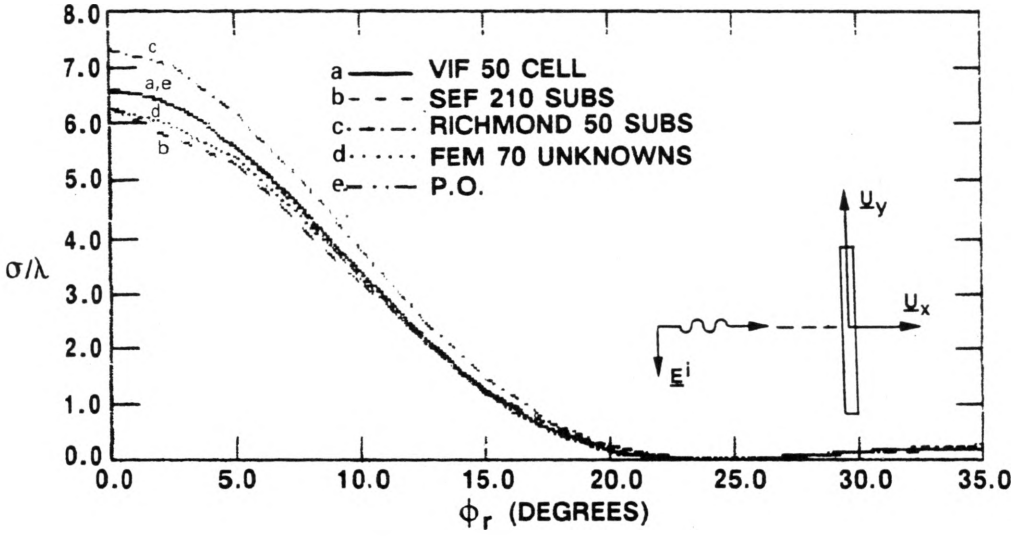

Figure 28. Bistatic Scattering Comparisons of a 50 Cell VIF, a 210 Subsection SEF, Richmond's Results, a FEM Solution with 70 Unknowns and a Physical Optics Solution for 0.05λ x 2.5λ Dielectric Slab

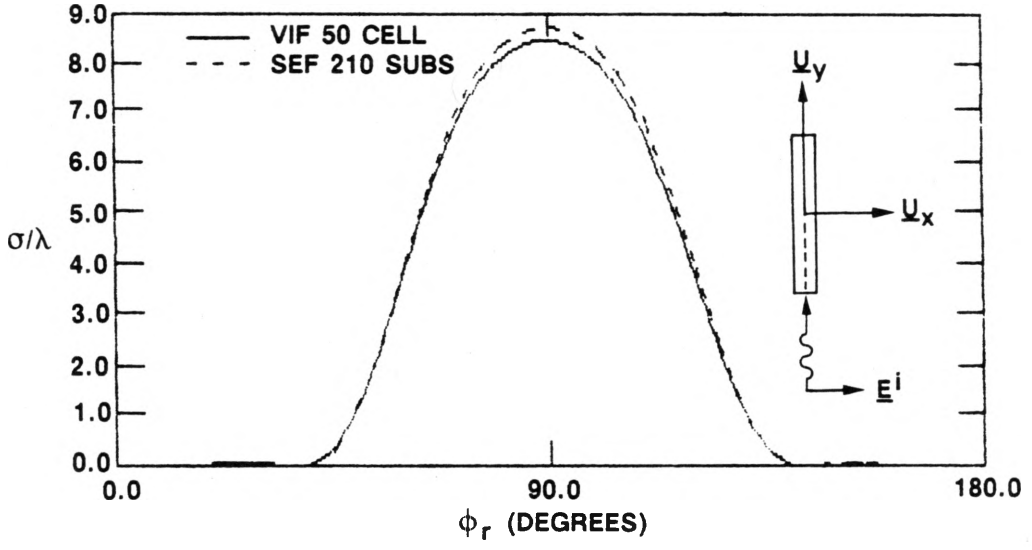

Figure 29. Bistatic Scattering Comparisons of a 50 Cell VIF and 210 Subsection SEF from 0.05λ x 2.5λ Dielectric (ϵ_r = 4.0) Slab. ϕ_i = 270°

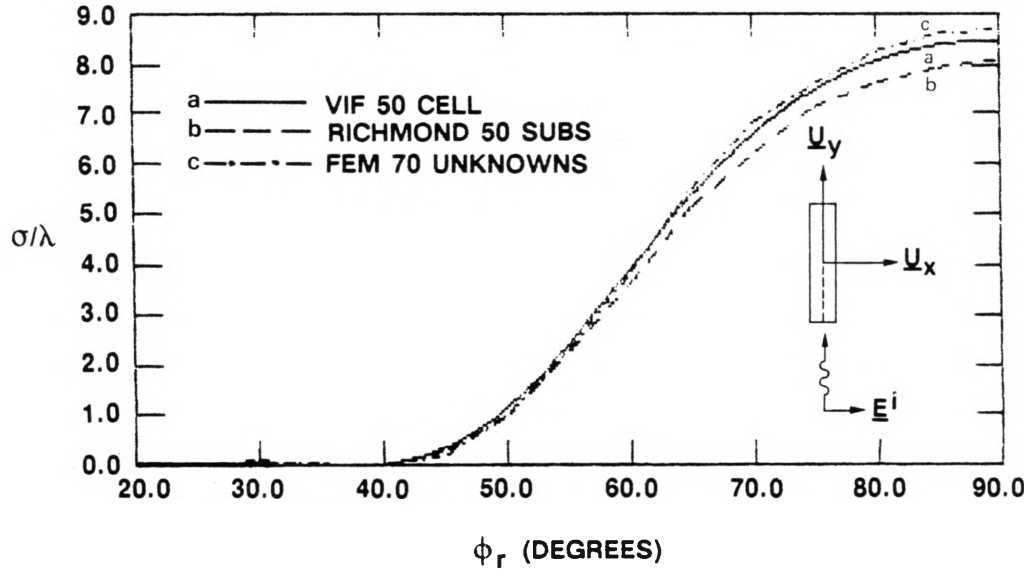

Figure 30. Bistatic Scattering Comparisons of a 50 Cell VIF, a FEM Solution with 70 Unknowns, and Richmond's Results using 50 Subsections for a 0.05λ x 2.5λ Dielectric Slab. ϕ_i = 270°

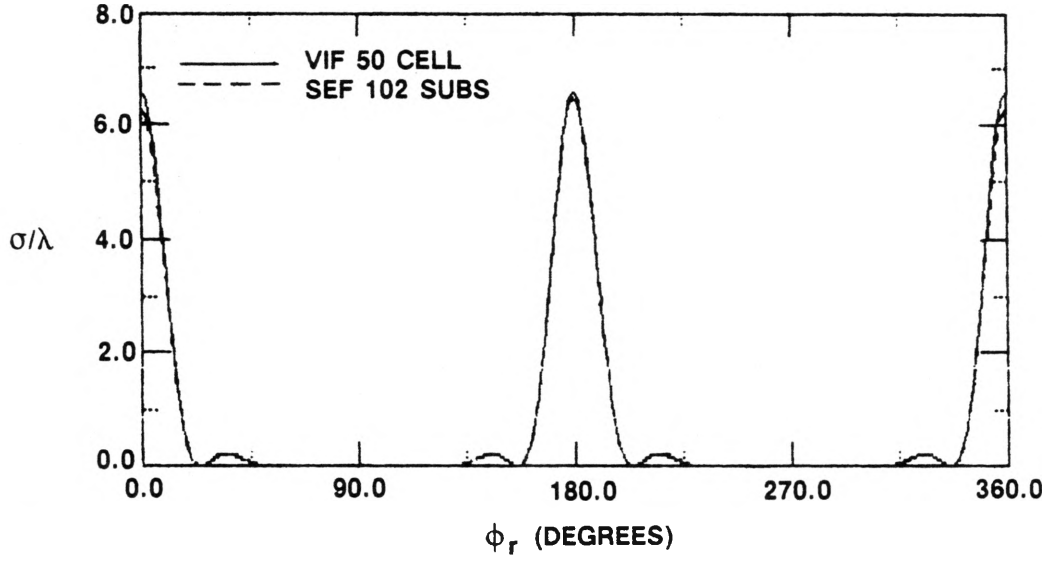

Figure 31. Bistatic Scattering (50 Cell VIF Compared with 102 Subsection SEF) from 0.05λ x 2.5λ Dielectric (ϵ_r = 4.0) Slab, ϕ_i = 180°

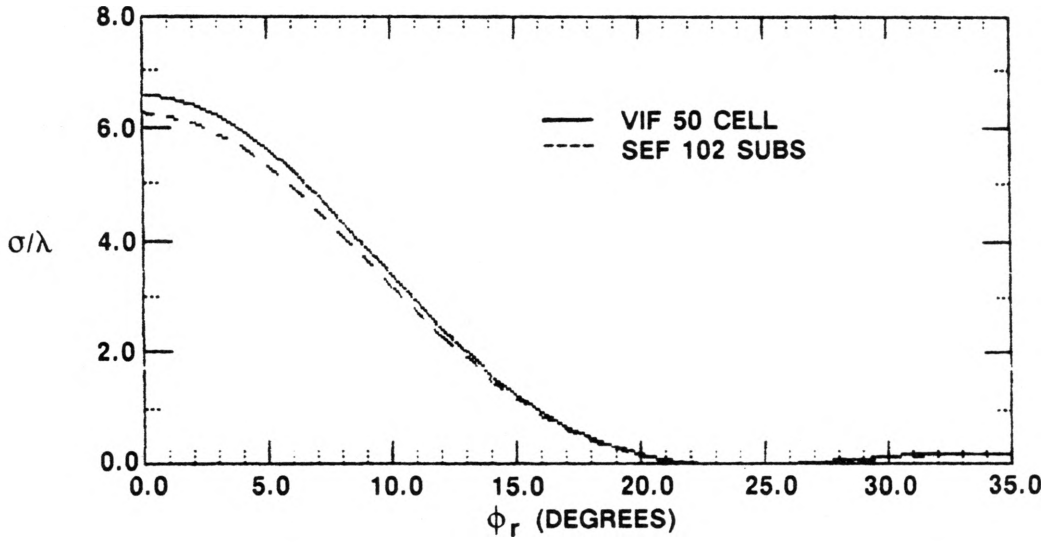

Figure 32. Bistatic Scattering (ϕ_i = 180°) of a 0.05λ x 2.5λ Dielectric (ϵ_r = 4.0) Slab Comparing a 50 Cell VIF with a 102 Subsection SEF Solution

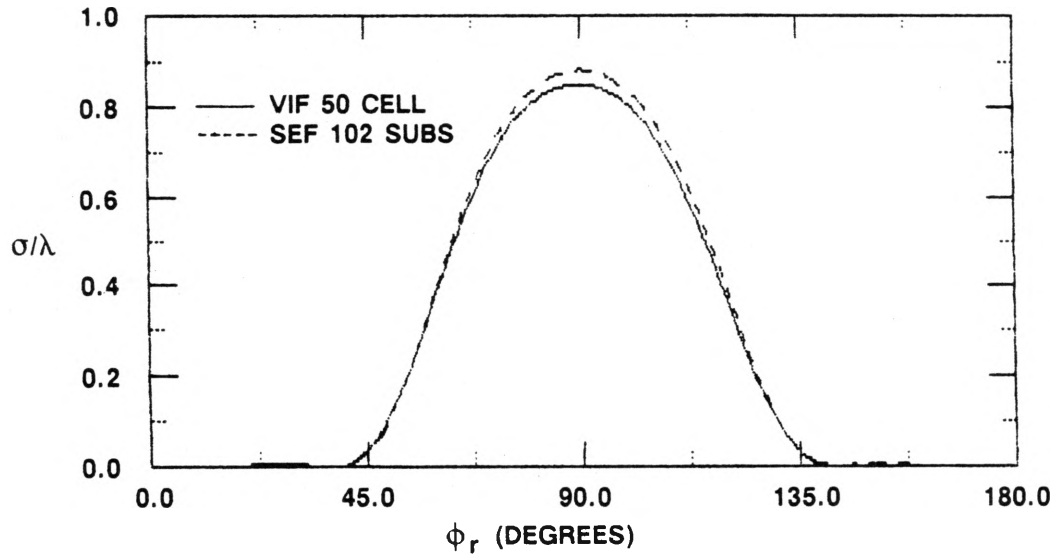

Figure 33. Bistatic Scattering (ϕ_i = 270°) from a 0.05λ x 2.5λ Dielectric (ϵ_r = 4.0) Slab Comparing a 50 Cell VIF with a 102 Subsection SEF Solution

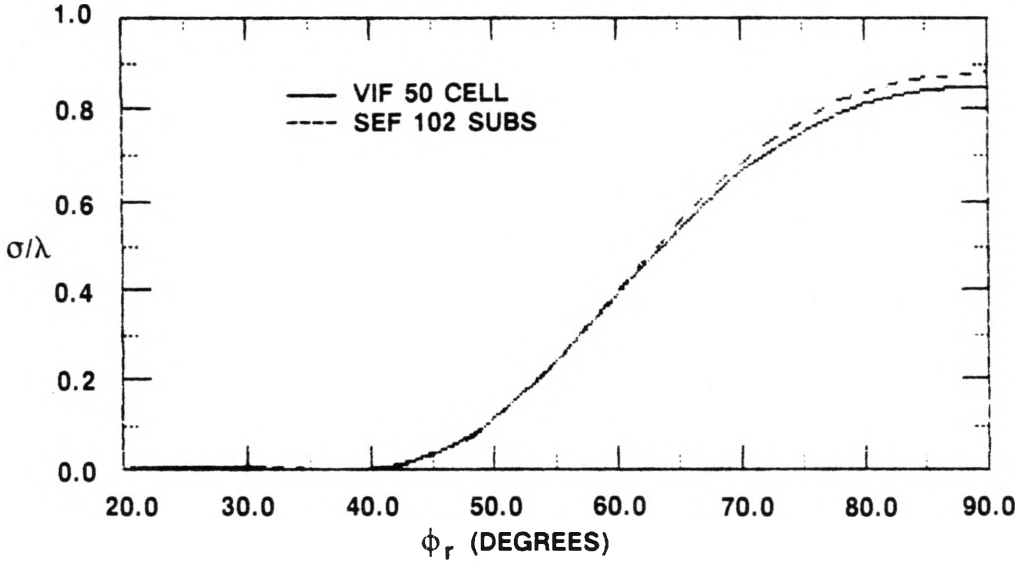

Figure 34. Bistatic Scattering (ϕ_i = 270°) from a 0.05λ x 2.5λ Dielectric (ϵ_r = 4.0) Slab Comparing a 50 Cell VIF with a 102 Subsection SEF Solution

6.0 SCATTERING FROM A THREE-DIMENSIONAL HOMOGENEOUS DIELECTRIC BODIES

For the three-dimensional problem of scattering from homogeneous dielectric bodies, the moment matrix equation (3.21) is used to calculate $\hat{Z}_{mn}$ given by (3.22). The simplest model to check the accuracy of this technique is a one cell cube with constant current expansions in $\underline{u}_x$, $\underline{u}_y$, and $\underline{u}_z$, as shown in Figure 35. The cube is centered at the origin of a Cartesian coordinate system and the expansion functions used in approximating $\underline{J}$ in (3.1) are

$$\underline{J}_n = \begin{cases} \underline{u}_x & n = 1 \\ \underline{u}_y & n = 2 \\ \underline{u}_z & n = 3 \end{cases} \tag{6.1}$$

These simple expansion functions have zero divergence in the dielectric volume. The modified impedance matrix elements $\hat{Z}_{mn}$ are evaluated from (3.22) for vector potential, scalar potential and displacement current terms.

6.1 Evaluation of Modified Impedance Matrix Elements

For the vector potential terms VP_{mn}, the symmetric product integral is approximated by evaluating the integrand at the center of the cube (m,n at the origin) and multiplying by the associated volume of the cube. The vector potential terms are evaluated from

$$VP_{mn} = j\omega \iiint_V \underline{J}_m \cdot \underline{A}_n \, dv \tag{6.2}$$

The inner integral of (6.2) is given by

$$\underline{A}_n = \underline{A}(\underline{J}_n) = \frac{\mu_o}{4\pi} \iiint_V \underline{J}_n \, \frac{e^{-jk|\underline{r}_m - \underline{r}_n'|}}{|\underline{r}_m - \underline{r}_n'|} \, dv' \tag{6.3}$$

where $|\underline{r}_m - \underline{r}_n'| = \sqrt{(x_m - x_n')^2 + (y_m - y_n')^2 + (z_m - z_n')^2}$.

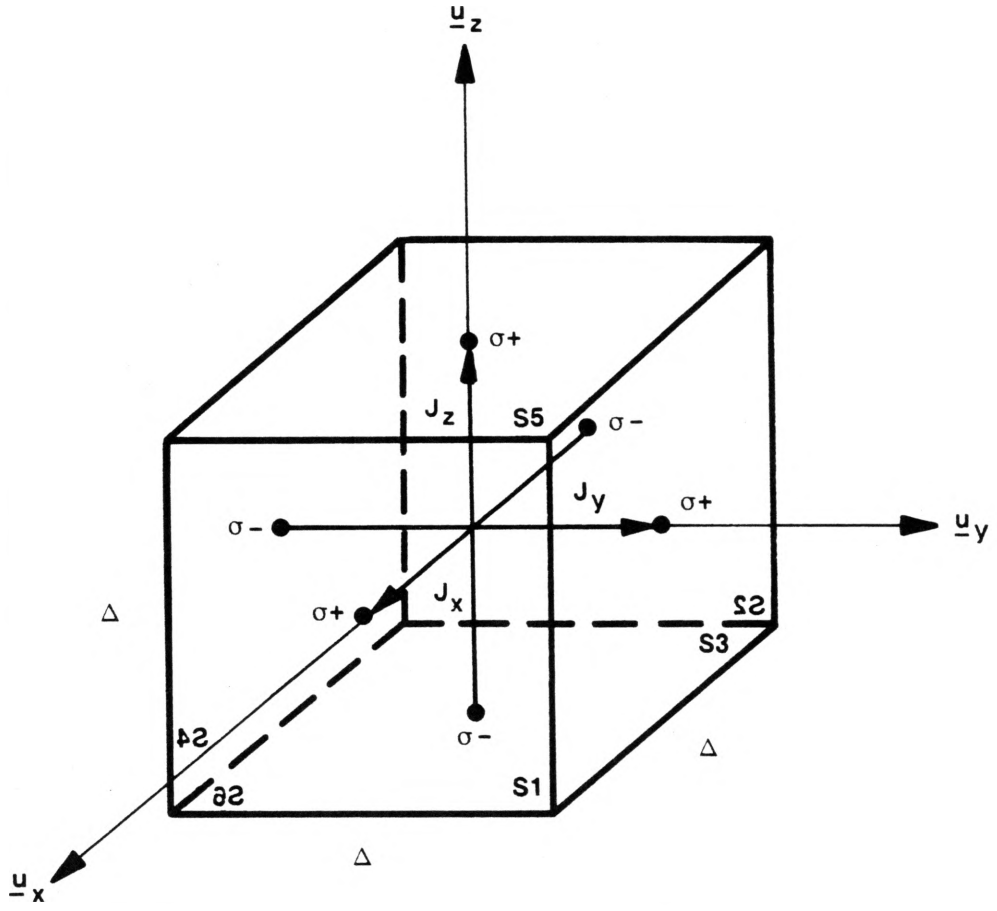

Figure 35. One Cell Model of Dielectric Cube (ϵ_r = 4.0) with Constant Expansions in $\underline{u}_x$, $\underline{u}_y$, and $\underline{u}_z$ and their Associated Charge Doublets

substitution of (6.3) into the vector potential integral term (6.2) gives

$$VP_{mn} = \frac{j\omega\mu_o}{4\pi} \left\{ \iiint_V \underline{J}_m \cdot \left[\iiint_V \underline{J}_n \frac{e^{-jk|\underline{r}_m - \underline{r}_n'|}}{|\underline{r}_m - \underline{r}_n'|} dv' \right] dv \right\} \qquad m = 1,2,3 \tag{6.4}$$

For single expansion functions in any one dimension, the only non-zero terms are the self-terms m=n. Orthogonal expansion functions do not contribute to the vector potential.

For m=n (self terms), the inner integral is evaluated at the center of the cube;

$$|\underline{r}_m - \underline{r}_n'| = \sqrt{x^2 + y^2 + z^2} = r' \tag{6.5}$$

An approximation of the resulting improper vector potential integral can be found by expanding the exponential in the integrand into a Maclaurin series [14] as

$$\frac{e^{-jkr'}}{r'} \cong \frac{1}{r'} - jk - \ldots \tag{6.6}$$

Substitution of (6.6) into (6.4) for m=n yields

$$\begin{aligned} VP_{mn} &= \frac{j\omega\mu_o}{4\pi} \iiint_V \underline{J}_m \cdot \left\{ \iiint_V \underline{J}_n \left(\frac{1}{r'} - jk \right) dv' \right\} dv \\ &= \frac{j\omega\mu_o}{4\pi} \iiint_V \underline{J}_m \cdot \underline{J}_n \left\{ \iiint_V \left(\frac{1}{r'} - jk \right) dv' \right\} dv \\ &= \frac{j\omega\mu_o \Delta^3}{4\pi} \iiint_V \left(\frac{1}{r'} - jk \right) dv' \qquad , m=n \end{aligned} \tag{6.7}$$

The integrand still has a $\frac{1}{r'}$ integrable volume singularity. This volume singularity can be approximated by a transformation of coordinates. A sphere of radius R with equal volume is used to replace the cubic volume (illustrated in Figure 36) as

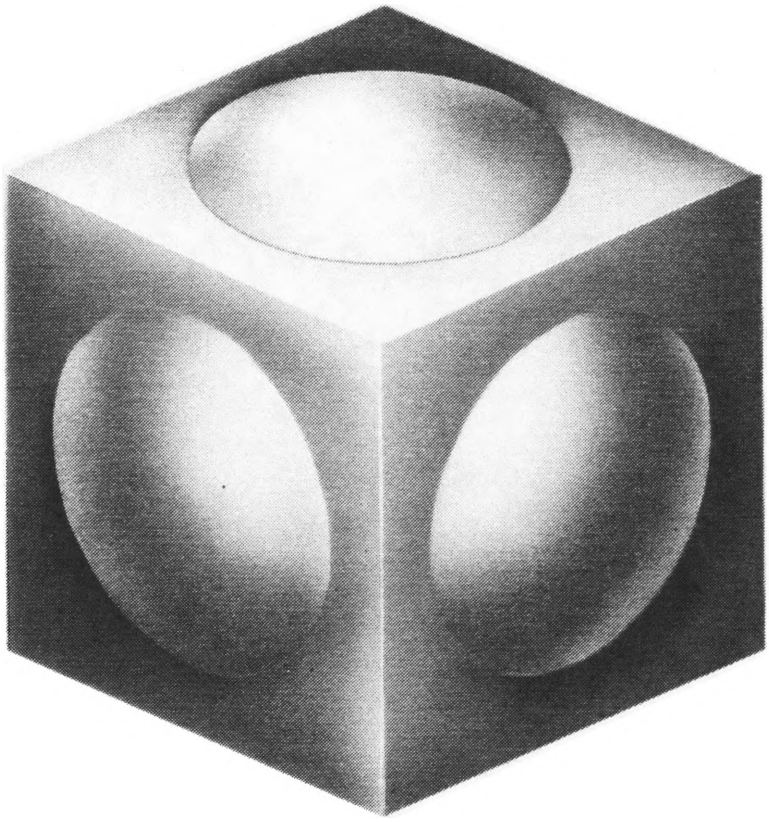

Figure 36. Spherical Volume Approximation to Cubic Cell Volume

$$V_{sphere} = V_{cube}$$
$$\frac{4\pi}{3} R^3 = \Delta^3 \tag{6.8}$$
$$R = \Delta \left(\frac{3}{4\pi}\right)^{1/3}$$

where R is the radius of the sphere. Transforming to spherical coordinates $dv' = r'^2 \sin\theta' dr' d\theta' d\phi'$, the integral (6.7) can be evaluated as

$$VP_{mn} = \frac{j\omega\mu_o \Delta^3}{4\pi} \int_0^{2\pi}\int_0^{\pi}\int_0^{R} \left(\frac{1}{r'} - jk\right) r'^2 \sin\theta' dr' d\theta' d\phi'$$
$$= \frac{j\omega\mu_o \Delta^5 \left(\frac{3}{4\pi}\right)^{2/3}}{2} + \frac{\omega\mu_o k \Delta^6}{4\pi} \qquad m=n \tag{6.9}$$

Therefore, the resulting vector potential terms are

$$VP_{mn} = \begin{cases} \dfrac{j\omega\mu_o \Delta^5 \left(\frac{3}{4\pi}\right)^{2/3}}{2} + \dfrac{\omega\mu_o k \Delta^6}{4\pi} & m=n \\ 0 & \text{otherwise} \end{cases} \tag{6.10}$$

Evaluation of the scalar potential terms involves the surface charge density doublet associated with each current expansion. Since the polarization current expansion functions begin and end on a surface, they give rise to a surface charge density (σ^+, σ^-) from (5.17) on surface centroids S_i and S_{i+1} as depicted in Figure 37. The surface charge is then expressed as

$$\sigma_n^+ = \frac{1}{j\omega} \quad \underline{r}' \text{ on } S_i \tag{6.11}$$

and

$$\sigma_n^- = \frac{-1}{j\omega} \quad \underline{r}' \text{ on } S_{i+1} \tag{6.12}$$

where n = 1, i = 1; n = 2, i = 3; and n = 3, i = 5.

From the current expansion $\underline{J}_n$ in each dimension, only one charge doublet is associated with each direction giving only self terms (m=n) for the scalar potential elements.

The scalar potential terms SP_{mn} are evaluated from equation (3.21) as

$$SP_{mn} = \iint_S \underline{n} \cdot \underline{J}_m \, \phi_n \, ds \tag{6.13}$$

The inner integral ϕ_n is actually in terms of two integrals resulting from the charge doublet associated with each current expansion function. This expression is given by

$$\phi_n = \phi(\sigma_n) = \frac{1}{4\pi\epsilon_o} \left\{ \iint_S \sigma_n^+(\underline{r}') \frac{e^{-jk|\underline{r}_m - \underline{r}'_{S_i}|}}{|\underline{r}_m - \underline{r}'_{S_i}|} \, ds' \right.$$

$$\left. + \iint_S \sigma_n^-(\underline{r}') \frac{e^{-jk|\underline{r}_m - \underline{r}'_{S_{i+1}}|}}{|\underline{r}_m - \underline{r}'_{S_{i+1}}|} \, ds' \right\} \qquad m = 1,2,3 \tag{6.14}$$

where $|\underline{r}_{S_i} - \underline{r}'_{S_{i+1}}| = |\underline{r}_{S_{i+1}} - \underline{r}'_{S_i}|$ in Figure 37 is the vector length between charges on the surface due to one current expansion. Substitution of (6.14) into the SP_{mn} integral term for the scalar potential terms m=n yields

$$SP_{mn} = \frac{1}{4\pi\epsilon_o} \left\{ \iint_S (\underline{n} \cdot \underline{J}_m) \left[\iint_S \sigma_n^+(\underline{r}') \frac{e^{-jk|\underline{r}_m - \underline{r}'_{S_i}|}}{|\underline{r}_m - \underline{r}'_{S_i}|} \, ds' \right.\right.$$

$$\left.\left. + \iint_S \sigma_n^-(\underline{r}') \frac{e^{-jk|\underline{r}_m - \underline{r}'_{S_{i+1}}|}}{|\underline{r}_m - \underline{r}'_{S_{i+1}}|} \, ds' \right] ds \right\} \qquad , m = n \tag{6.15}$$

Integration gives

$$SP_{mn} = \frac{\Delta^2}{4j\omega\epsilon_o\pi} \left\{ \iint_S \frac{e^{-jk|\underline{r}_{S_i} - \underline{r}'_{S_i}|}}{|\underline{r}_{S_i} - \underline{r}'_{S_i}|} \, ds' \right.$$

$$- \iint_S \frac{e^{-jk|\underline{r}_{S_i} - \underline{r}'_{S_{i+1}}|}}{|\underline{r}_{S_i} - \underline{r}'_{S_{i+1}}|} \, ds'$$

$$\left. - \iint_S \frac{e^{-jk|\underline{r}_{S_{i+1}} - \underline{r}'_{S_i}|}}{|\underline{r}_{S_{i+1}} - \underline{r}'_{S_i}|} \, ds' + \iint_S \frac{e^{-jk|\underline{r}_{S_{i+1}} - \underline{r}'_{S_{i+1}}|}}{|\underline{r}_{S_{i+1}} - \underline{r}'_{S_{i+1}}|} \, ds' \right\} , m = n \tag{6.16}$$

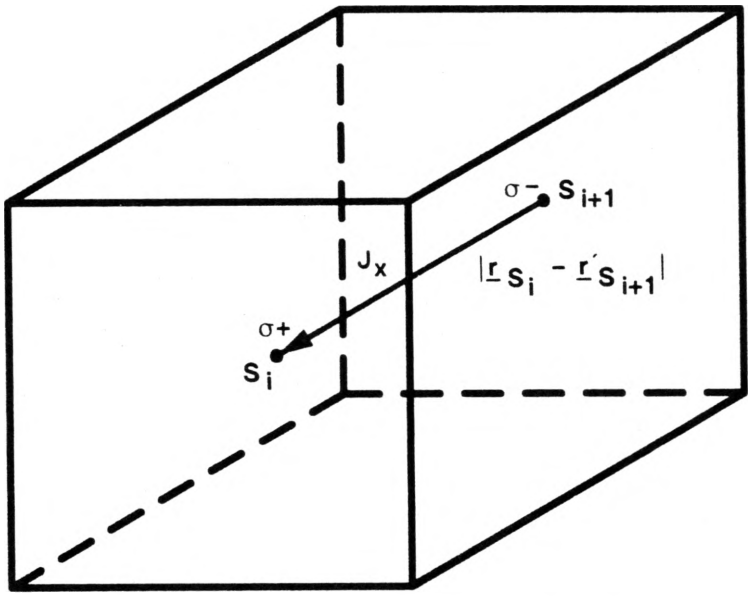

Figure 37. Local Coordinates for Centroid Source Point σ^-_n and Observation Point σ^+_n in Scalar Potential Self Terms

The scalar potential terms involve two types of integrals, one type where $|\underline{r} - \underline{r}'| \to 0$ and the other type where $|\underline{r} - \underline{r}'| = \Delta$. For the first and last integrals in (6.16), the Maclaurin series approximation to the integrand as $|\underline{r} - \underline{r}'| \to 0$ given by (6.6) is used; this results in

$$\iint_S \frac{e^{-jk|\underline{r} - \underline{r}'|}}{|\underline{r} - \underline{r}'|}\, ds' \cong \iint_S \left(\frac{1}{r'} - jk\right) ds'$$

$$= 8\left(\frac{\Delta}{2}\right) \log\left(1 + \sqrt{2}\right) - jk\Delta^2 \qquad , m = n \tag{6.17}$$

Evaluation of the surface integral $\frac{1}{r'}$, in the xy, xz, or zy area is given in Appendix B (B.6) where $|\underline{r} - \underline{r}'| = r'$ at the surface centroids S_i and S_{i+1}.

For $|\underline{r} - \underline{r}'| = \Delta$, m=n, an approximation for large r is used for the second and third integrations yielding

$$\iint_S \frac{e^{-jk|\underline{r} - \underline{r}'|}}{|\underline{r} - \underline{r}'|}\, ds' \cong \frac{e^{-jk\Delta}}{\Delta} \iint_S ds' = \Delta\, e^{-jk\Delta} \qquad , m = n \tag{6.18}$$

Substitution of (6.17) and (6.18) into equation (6.16) for the scalar potential terms results in

$$SP_{mn} = \frac{\Delta^2}{4j\omega\epsilon_o\pi}\left\{16\left(\frac{\Delta}{2}\right)\log\left(1 + \sqrt{2}\right) - 2\, jk\Delta^2 - 2\Delta\, e^{-jk\Delta}\right\} \quad , m = n \tag{6.19}$$

Since each constant current expansion function produces a charge doublet, the non-self scalar potential terms add to zero for this single cubic model. This is depicted in Figure 38 showing the equal vector lengths between doublets for any two current expansions. The resulting scalar potential matrix elements are

$$SP_{mn} = \begin{cases} \frac{\Delta^2}{4j\omega\epsilon_o\pi}\left[16\left(\frac{\Delta}{2}\right)\log\left(1 + \sqrt{2}\right) - 2\, jk\Delta^2 - 2\Delta\, e^{-jk\Delta}\right] & m = n \\ 0 & m \neq n \end{cases} \tag{6.20}$$

Evaluation of the displacement current elements S_{mn} from (3.20) gives nonzero elements only for self terms, due to the orthogonality of expansion functions. The displacement current integral terms can be written as

$$S_{mn} = \frac{1}{j\omega\epsilon_o(\epsilon_r - 1)} \iiint_V \underline{J}_m \cdot \underline{J}_n\, dv \tag{6.21}$$

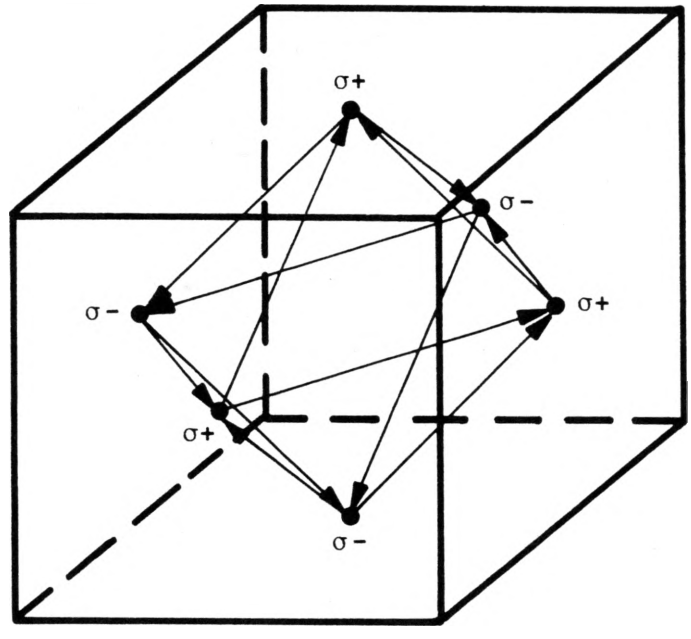

Figure 38. Local Coordinate Vector Lengths for Source and Observation Points at the Centroids of the Surfaces for Non-Self Scalar Potential Terms

and evaluation of all matrix elements results in

$$S_{mn} = \begin{cases} \dfrac{\Delta^3}{j\omega\epsilon_o(\epsilon_r - 1)} & m=n \\ 0 & m \neq n \end{cases} \tag{6.22}$$

The modified impedance matrix $[\hat{Z}_{mn}]$ can be obtained from (3.21) by summation of (6.10), (6.20), and (6.22).

6.2 Discussion of Numerical Results of Three-Dimensional Scattering from a Dielectric Cube

The bistatic scattering formula is given by

$$\sigma_B = \frac{\eta^2 k^2}{4\pi} \left| \left[\tilde{V}_m^r\right] \left[\hat{Z}_{mn}^{-1}\right] \left[V_m^i\right] \right|^2 \tag{6.23}$$

as derived in Appendix C using the reciprocity relationship for three dimensional problems.

Solving for σ_B (C.20) using the modified impedance moment matrix $[\hat{Z}_{mn}]$, the bistatic radar cross section in E_θ from a tenth of a wavelength homogeneous dielectric ($\epsilon_r = 4.0$) cube was computed with a uniform incident wave at $\theta_i = 180°$, $\phi_i = 0°$, and $\phi_r = 0°$. Figure 39 is a plot of this solution using three unknowns compared to a SEF using 312 unknowns. A dipole pattern is obtained in E_θ where no variation in the backscattered ($\theta_r = 180°$) and forward scattered ($\theta_r = 0°$) field is obtained due to the simple expansion functions used. The scattering in E_ϕ versus θ_r at $\phi_r = 90°$ is a constant. The VIF solution differs by only 5.6 percent from the SEF solution at $\theta_r = 180°$ in the backscatter direction. The forward scattered solution can be improved by increasing the number of current expansions in the VIF.

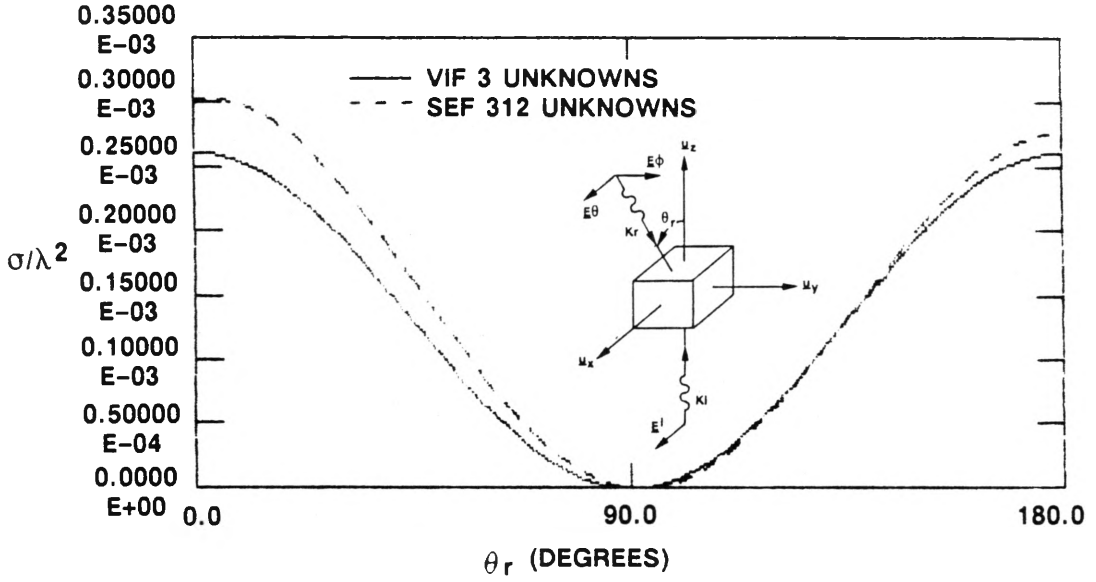

Figure 39. Bistatic Scattering (ϕ_i = 0°, θ_i = 180°) in E_θ for 0.1λ Dielectric (ϵ_r = 4.0) Cube Comparing a VIF Using Three Unknowns with a SEF Using 312 Unknowns

Fig 3

7.0 CONCLUSIONS

A volume integral formulation has been presented for computing the electromagnetic scattering from homogeneous dielectric bodies modeled using square cells for the two–dimensional case and cubic cells for the three–dimensional case. The complexity of present printed circuit antennas and scatterers has increased the need for computer aided design (CAD) tools for dynamic electromagnetic analysis. With the next generation computer memory storage, large matrices can be solved efficiently for more complex problems. In this formulation, the method of moments is used to generate an impedance matrix equation which can be used to solve for the scattered or radiated field. Computation time is reduced by approximating each non–self integral in the vector potential and scalar potential terms by the value of the integrand at the center of the subsection times the length, area, or volume of the subsection. An accurate determination of the near fields is obtained by modeling the surface charge density accurately. For thin homogeneous dielectric substrates used in printed circuit applications, expansion functions are chosen to produce no volume charge density. This results in surface charge related to terminating volume polarization currents. These charges are formed in doublets of uniform surface density, σ^+ and σ^-, arising from each current expansion function. The size of the resulting modified impedance matrix and the number of unknowns is equal to the number of current loops minus one. The reduction of the operator equation from an integro–differential equation to an integral equation is an important simplification which directly reduces the complexity of the solution. The enforcement of the equation of continuity in the homogeneous volume specifically constrains the volume charge density to be zero. This formulation differs from those described in [4,5, and 6] by the resulting integral operator equation and the equation of continuity being strictly satisfied in the volume with the proper choice of expansion functions.

The volume integral approach presented here is shown to be an accurate method of modeling cubic bodies and two–dimensional bodies which are representable as a summation of square cells. The comparison of numerical results between this solution and others, namely the surface equivalence formulation solutions, shows good agreement while using fewer unknowns and simpler expansion functions in the volume integral formulation. To obtain variation in the forward and backscattered field in E_θ and E_ϕ in the three–dimensional model, non–constant expansion functions need to be used as was done in the two–dimensional square post model. Examples of non–constant expansion functions which satisfy the equation of continuity in the dielectric volume are depicted in Figure 40. This three–dimensional model adopts the circulating current loops as developed in the two–dimensional case for modeling with more than one cell in a linear dimension.

This formulation can be extended to model inhomogeneous bodies using the surface charge density doublet representation and enforcing the continuity of tangential $\underline{E}$ across the material boundaries. For more complex objects involving curved layered shapes, a prismatic cell model needs to be developed. A method for composite (dielectric and conductors) models can be formulated using surface conduction currents $\underline{J}_c$ and the free charges σ_c on the conductors to generate a coupled set of matrix equations. This extension of the formulation can then be used to solve for the radiated and scattered fields for printed circuit antenna problems.

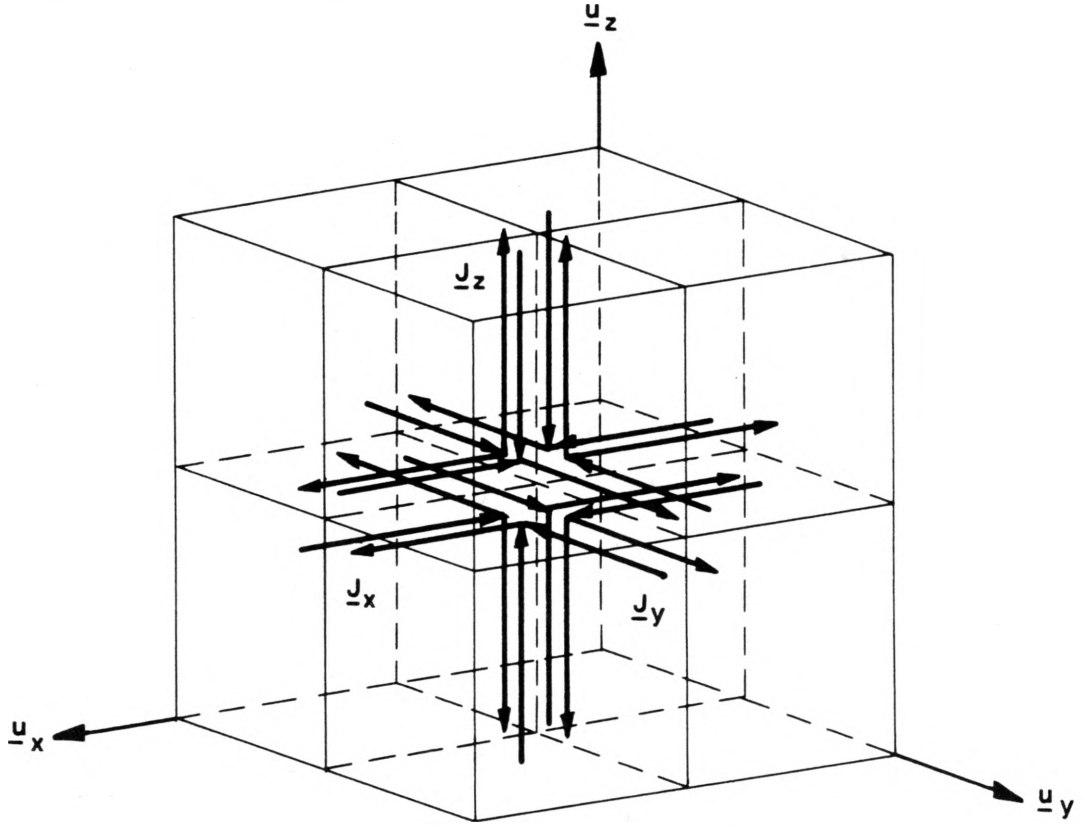

Figure 40. Eight Quarter Circulating Current Loops Defined in a Cubic Cell Volume

Fig 4

APPENDIX A

A.1 TE BISTATIC RADAR CROSS SECTION IN TWO DIMENSIONS

The bistatic radar cross section σ_B is given by

$$\sigma_B = 2\pi\rho \left| \frac{\underline{E}^s}{\underline{E}^i} \right|^2 \tag{A.1}$$

where ρ is the radius in polar coordinates. Figure A1 gives the geometry of a two-dimensional dielectric body in the presence of a test dipole incident field. The scattered field can be determined from reciprocity. Letting the incident field $\underline{E}^i$ equal a unit plane wave

$$\sigma_B = 2\pi\rho \left| \underline{E}^s \right|^2 \tag{A.2}$$

The test dipole $I\ell_r$ at the receiving point is adjusted to produce a unit plane wave at the scatterer where

$$\underline{E}^r = \underline{u}_r \, e^{-j\underline{k}_r \cdot \underline{\rho}_n}, \qquad \underline{u}_r = -\underline{u}_x \sin\phi_r + \underline{u}_y \cos\phi_r \tag{A.3}$$

and

$$\underline{E}^i = \underline{u}_i \, e^{-j\underline{k}_i \cdot \underline{\rho}_n}, \qquad \underline{u}_i = -\underline{u}_x \sin\phi_i + \underline{u}_y \cos\phi_i \tag{A.4}$$

in rectangular coordinates.

$\underline{E}^i$ is the incident transmitted field where $\underline{u}_r$ and $\underline{u}_i$ are the unit vectors specifying the polarization of the wave. The wave numbers $\underline{k}_r$ and $\underline{k}_i$ are pointing in the direction of the travel and $\underline{\rho}_n$ is the radius vector to the point n on the scatterer. Moving the test dipole to infinity and using the reciprocity relationship between sources and fields at 1 and 2

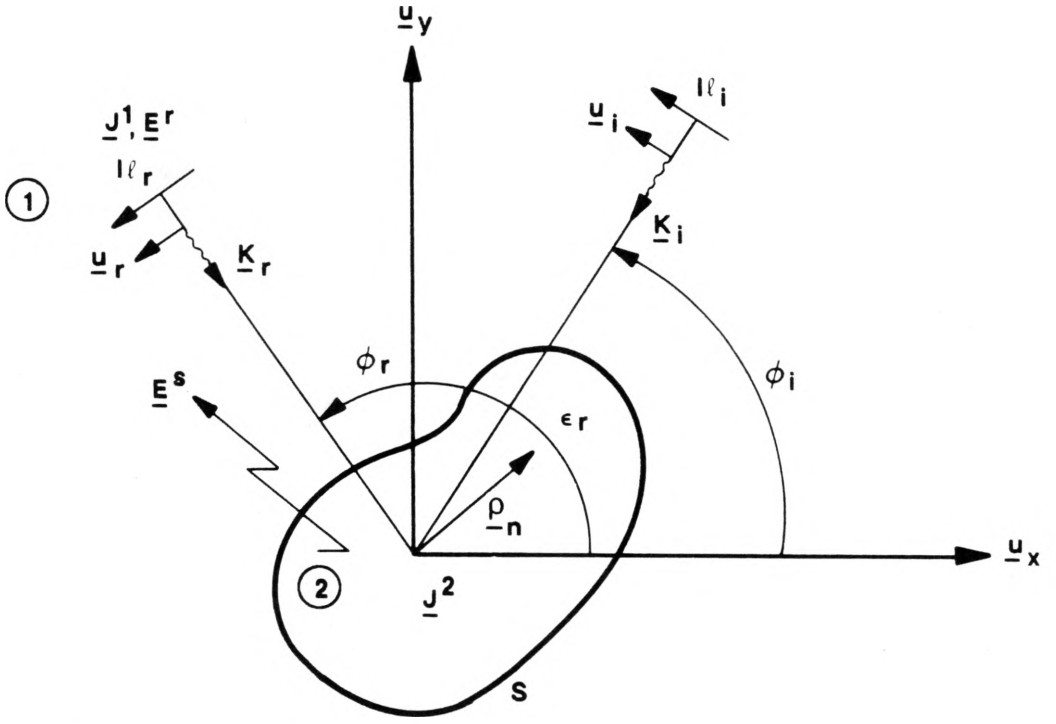

Figure A1. Two–Dimensional Coordinates for Incident and Receiving Test Dipoles in Reciprocity Relationship

$$\int_{\ell'} \underline{J}^1 \cdot \underline{E}^s \, d\ell' = \iint_S \underline{J}^2 \cdot \underline{E}^r \, ds'$$

$$I\ell_r \, E^s = \iint_S \underline{J}^2 \cdot \underline{E}^r \, ds'$$

$$E^s = \frac{1}{I\ell_r} \iint_S \underline{J}^2 \cdot \underline{E}^r \, ds' \tag{A.5}$$

where E^s is the $\underline{u}_r$ component of $\underline{E}$ from the body and $\underline{J}^2$ is the polarization current in the body. The constant $\frac{1}{I\ell_r}$ is needed to produce a plane wave of unit amplitude at the origin. Figure A2 shows the far field relationship between source and field.
In the far zone

$$|\underline{\rho} - \underline{\rho}'| \cong \rho - \rho' \cos\theta \tag{A.6}$$

is the phase term and

$$|\underline{\rho} - \underline{\rho}'| \cong \rho \tag{A.7}$$

is the amplitude term.

The far field electric component for the dipole is

$$E_\phi = -j\omega A_\phi \tag{A.8}$$

where the magnetic vector potential of the test dipole $I\ell_r$ is given by

$$A_\phi = \frac{I\ell_r \mu_o}{4j} H_o^{(2)} (k \, |\underline{\rho} - \underline{\rho}'|) \tag{A.9}$$

As the radius goes to infinity, we use the large-argument formulas from the Hankel function of the second kind [8]

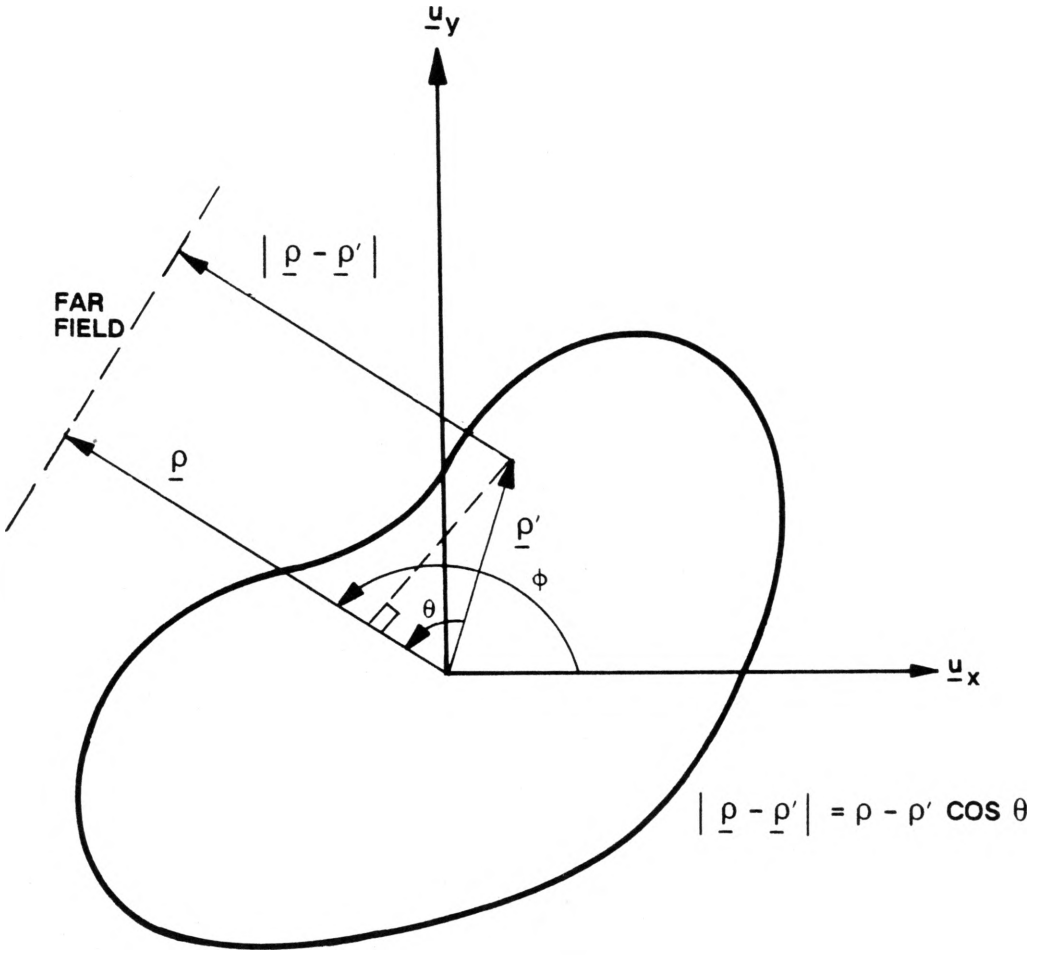

Figure A2. Coordinates for Far Field Source and Observation Points in Two Dimensions

$$H_o^{(2)}\,(k\,|\underline{\rho}-\underline{\rho}'|) \xrightarrow[|\underline{\rho}-\underline{\rho}'|\to\infty]{} \sqrt{\frac{2j}{\pi k\,|\underline{\rho}-\underline{\rho}'|}}\; j^{o}\; e^{-jk|\underline{\rho}-\underline{\rho}'|}$$

$$\cong \sqrt{\frac{2j}{\pi k\rho}}\; e^{-jk\,(\rho\,-\,\rho'\cos\theta)} \tag{A.10}$$

Substitution of (A.10) into (A.9) gives

$$A_\phi = \frac{I\ell_r\mu_o}{4j}\sqrt{\frac{2j}{\pi k\rho}}\; e^{-jk\rho}\, e^{+jk\rho'\cos\theta} \tag{A.11}$$

The far field is then solved by substitution of (A.11) into (A.8) yielding

$$E_\phi = -j\omega A_\phi = \frac{-I\ell_r\mu_o\omega}{4}\sqrt{\frac{2j}{\pi k\rho}}\; e^{-jk\rho}\, e^{+jk\rho'\cos\theta} \tag{A.12}$$

Setting the amplitude term to unity

$$\frac{-I\ell_r\mu_o\omega}{4}\sqrt{\frac{2j}{\pi k\rho}}\; e^{-jk\rho} = 1$$

$$\frac{1}{I\ell_r} = \frac{-\omega\mu_o}{4}\sqrt{\frac{2j}{\pi k\rho}}\; e^{-jk\rho} \tag{A.13}$$

The scattered field is determined from substitution of (A.13) into (A.5) resulting in

$$E^s = \frac{-\omega\mu_o}{4}\sqrt{\frac{2j}{\pi k\rho}}\; e^{-jk\rho}\iint_S \underline{J}^2 \cdot \underline{E}^r\, ds' \tag{A.14}$$

A numerical approximation to the integral in (A.14) is obtained by defining a voltage receiving matrix from (3.8) as follows:

$$V_m^r = \langle \underline{J}_m, \underline{E}^r \rangle$$

$$= \iint_S \underline{J}_m \cdot \underline{E}^r\, ds'$$

$$= \frac{1}{2}\iint_S \left(\underline{u}_x \ell P(x')\, P(y') + p\underline{u}_y\, P(y')\, P(x') \right) \cdot \underline{u}_r\, e^{-j\underline{k}_r \cdot \underline{\rho}_n}\, dx'\, dy'$$

$$= \frac{1}{2} \iint_S \left(\underline{u}_x \ell P(x') P(y') + p\underline{u}_y P(y') P(x') \right)$$

$$\cdot \left(-\underline{u}_x \sin \phi_r + \underline{u}_y \cos \phi_r \right) e^{-j\underline{k}_r \cdot \underline{\rho}_n} \, dx' \, dy'$$

$$= \frac{\Delta^2}{2} e^{-j\underline{k}_r \cdot \underline{\rho}_n} \left(-\ell \sin \phi_r + p \cos \phi_r \right) \tag{A.15}$$

where $\ell = -1$, m=1, 4; $\ell = 1$, m=2, 3; p = 1, m=1, 2; p = −1, m=3, 4.

Further approximation of (A.14) as the matrix product gives

$$E^s = \frac{-\omega\mu_o e^{-jk\rho}}{4} \sqrt{\frac{2j}{\pi k\rho}} \left[\tilde{V}_m^r \right] \left[I_n \right] \tag{A.16}$$

where $[\tilde{V}_m^r]$ is the transpose of $[V_m^r]$ and $[I_n]$ is given by (3.29) with

$$V_m^i = \left\langle \underline{J}_m, \underline{E}^i \right\rangle$$

$$= \iint_S \underline{J}_m \cdot \underline{E}^i \, ds'$$

$$= \frac{\Delta^2}{2} e^{-j\underline{k}_i \cdot \underline{\rho}_n} \left(-\ell \sin \phi_i + p \cos \phi_i \right) \begin{cases} \ell = -1 & m=1,4 \\ \ell = 1 & m=2,3 \\ p = 1 & m=1,2 \\ p = -1 & m=3,4 \end{cases} \tag{A.17}$$

Therefore (A.16) becomes

$$E^s = \frac{-\omega\mu_o e^{-jk\rho}}{4} \sqrt{\frac{2j}{\pi k\rho}} \left[\tilde{V}_m^r \right] \left[\hat{Z}_{mn}^{-1} \right] \left[V_m^i \right] \tag{A.18}$$

Substitution of (A.18) into (A.2) for the bistatic radar cross section results in

$$\sigma_B = 2\pi\rho \left| \frac{-\omega\mu_o e^{-jk\rho}}{4} \sqrt{\frac{2j}{\pi k\rho}} \left[\tilde{V}_m^r \right] \left[\hat{Z}_{mn}^{-1} \right] \left[V_m^i \right] \right|^2$$

$$= \frac{\mu_o^2 \omega^2}{4k} \left| \left[\tilde{V}_m^r \right] \left[\hat{Z}_{mn}^{-1} \right] \left[V_m^i \right] \right|^2 \tag{A.19}$$

APPENDIX B

B.1 EVALUATION OF TWO-DIMENSIONAL SURFACE INTEGRAL

Surface integrals of the form

$$\iint_S \frac{1}{r'}\, ds' \tag{B.1}$$

can be evaluated over a square surface area. Assuming a square of width and length Δ centered at the origin of the x, y coordinates, the integral (B.1) can be rewritten as

$$\int_{\frac{-\Delta}{2}}^{\frac{\Delta}{2}} \int_{\frac{-\Delta}{2}}^{\frac{\Delta}{2}} \frac{1}{\sqrt{x^2+y^2}}\, dx\, dy = \int_{\frac{-\Delta}{2}}^{\frac{\Delta}{2}} \left[\log\left(x + \sqrt{x^2+y^2}\right)\Big|_{\frac{-\Delta}{2}}^{\frac{\Delta}{2}}\right] dy$$

$$= \int_{\frac{-\Delta}{2}}^{\frac{\Delta}{2}} \log\left[\frac{\Delta}{2} + \sqrt{\left(\frac{\Delta}{2}\right)^2 + y^2}\,\right] dy - \int_{\frac{-\Delta}{2}}^{\frac{\Delta}{2}} \log\left[\frac{-\Delta}{2} + \sqrt{\left(\frac{\Delta}{2}\right)^2 + y^2}\,\right] dy \tag{B.2}$$

Letting

$$u = \log\left(\frac{\Delta}{2} + \sqrt{\left(\frac{\Delta}{2}\right)^2 + y^2}\right)$$

$$du = \frac{1}{\frac{\Delta}{2} + \sqrt{\left(\frac{\Delta}{2}\right)^2 + y^2}} \left(\frac{1}{2}\left(\left(\frac{\Delta}{2}\right)^2 + y^2\right)^{-1/2} 2y\right) dy \tag{B.3}$$

in the first integral and letting

$$u' = \log\left(-\frac{\Delta}{2} + \sqrt{\left(\frac{\Delta}{2}\right)^2 + y^2}\right)$$

$$du' = \frac{1}{-\frac{\Delta}{2} + \sqrt{\left(\frac{\Delta}{2}\right)^2 + y^2}} \left(\frac{1}{2}\left(\left(\frac{\Delta}{2}\right)^2 + y^2\right)^{-1/2} 2y\right) dy \tag{B.4}$$

in the second integral and making the change of variables into (B.2) integrating by parts results in two new integrals

$$\int_{\frac{-\Delta}{2}}^{\frac{\Delta}{2}} \int_{\frac{-\Delta}{2}}^{\frac{\Delta}{2}} \frac{1}{\sqrt{x^2+y^2}}\, dx\, dy = \frac{\Delta}{2} \log\left(\frac{\Delta}{2} + \sqrt{\left(\frac{\Delta}{2}\right)^2 + y^2}\right)\Bigg|_{\frac{-\Delta}{2}}^{\frac{\Delta}{2}}$$

$$- \int_{\frac{-\Delta}{2}}^{\frac{\Delta}{2}} \frac{y2}{\left(\frac{\Delta}{2} + \sqrt{\left(\frac{\Delta}{2}\right)^2 + y2}\right)\left(\sqrt{\left(\frac{\Delta}{2}\right)^2 + y2}\right)}\, dy$$

$$- \frac{\Delta}{2} \log\left(\frac{-\Delta}{2} + \sqrt{\left(\frac{\Delta}{2}\right)^2 + y2}\right)\Bigg|_{\frac{-\Delta}{2}}^{\frac{\Delta}{2}}$$

$$+ \int_{\frac{-\Delta}{2}}^{\frac{\Delta}{2}} \frac{y2}{\left(\frac{-\Delta}{2} + \sqrt{\left(\frac{\Delta}{2}\right)^2 + y2}\right)\left(\sqrt{\left(\frac{\Delta}{2}\right)^2 + y2}\right)}\, dy \qquad \text{(B.5)}$$

Multiplication of the top and bottom of the first integrand by $\left(\frac{-\Delta}{2} + \sqrt{\left(\frac{\Delta}{2}\right)^2 + y2}\right)$ and the second integrand by $\left(\frac{\Delta}{2} + \sqrt{\left(\frac{\Delta}{2}\right)^2 + y2}\right)$ in equation (B.5) yields

$$= 2\,\frac{\Delta}{2} \log\left(\frac{\Delta}{2}\left(1+\sqrt{2}\right)\right) + \int_{\frac{-\Delta}{2}}^{\frac{\Delta}{2}} \frac{\left(\frac{\Delta}{2} - \sqrt{\left(\frac{\Delta}{2}\right)^2 + y2}\right)}{\sqrt{\left(\frac{\Delta}{2}\right)^2 + y2}}\, dy$$

$$- 2\,\frac{\Delta}{2} \log\left(\frac{\Delta}{2}\left(-1+\sqrt{2}\right)\right) + \int_{\frac{-\Delta}{2}}^{\frac{\Delta}{2}} \frac{\left(\frac{\Delta}{2} + \sqrt{\left(\frac{\Delta}{2}\right)^2 + y2}\right)}{\sqrt{\left(\frac{\Delta}{2}\right)^2 + y2}}\, dy$$

$$= \Delta \log\left(\frac{\Delta}{2}\left(1+\sqrt{2}\right)\right) - \Delta \log\left(\frac{+\Delta}{2}\left(-1+\sqrt{2}\right)\right)$$

$$+ \frac{\Delta}{2} \log\left(\frac{\Delta}{2} + \sqrt{2\left(\frac{\Delta}{2}\right)^2}\right) - \frac{\Delta}{2} \log\left(\frac{-\Delta}{2} + \frac{\Delta}{2}\sqrt{2}\right) - \Delta$$

$$+ \frac{\Delta}{2} \log\left(\frac{\Delta}{2} + \frac{\Delta}{2}\sqrt{2}\right) - \frac{\Delta}{2} \log\left(\frac{-\Delta}{2} + \frac{\Delta}{2}\sqrt{2}\right) + \Delta$$

$$= \Delta \log\left(\frac{\Delta}{2}\left(1+\sqrt{2}\right)\right) - \Delta \log\left(\frac{\Delta}{2}\left(-1+\sqrt{2}\right)\right)$$

$$+ \frac{\Delta}{2} \log\left(\frac{\Delta}{2}\left(1+\sqrt{2}\right)\right) - \frac{\Delta}{2} \log\left(\frac{\Delta}{2}\left(-1+\sqrt{2}\right)\right) - \Delta$$

$$+ \frac{\Delta}{2} \log\left(\frac{\Delta}{2}\left(1+\sqrt{2}\right)\right) - \frac{\Delta}{2} \log\left(\frac{\Delta}{2}\left(-1+\sqrt{2}\right)\right) + \Delta$$

$$= 2\Delta \log\left(\frac{\Delta}{2}\left(1+\sqrt{2}\right)\right) - 2\Delta \log\left(\frac{\Delta}{2}\left(-1+\sqrt{2}\right)\right)$$

$$= 2\Delta \log\left(\frac{\Delta}{2}\right) + 2\Delta \log\left(1+\sqrt{2}\right) - 2\Delta \log\left(\frac{\Delta}{2}\right) - 2\Delta \log\left(-1+\sqrt{2}\right)$$

$$= 4\Delta \log\left(1+\sqrt{2}\right) \qquad \text{(B.6)}$$

APPENDIX C

C.1 BISTATIC RADAR CROSS SECTION FOR THREE-DIMENSIONAL SCATTERING

The bistatic radar cross section σ_B is given by

$$\sigma_B = 4\pi r^2 \left| \frac{\underline{E}^s}{\underline{E}^i} \right|^2 \tag{C.1}$$

in three-dimensions where r is the radius in spherical coordinates. Figure C1 shows the geometry of a three-dimensional dielectric cube in the presence of a test dipole incident field. The scattered field can be determined from reciprocity. Setting the incident field $\underline{E}^i$ equal to a unit plane wave

$$\sigma_B = 4\pi r^2 \left| \underline{E}^s \right|^2 \tag{C.2}$$

The test dipole $I\ell_r$ at the receiving point is adjusted to produce a unit plane wave at the scatterer. The electric field produced by $I\ell_r$ is

$$\underline{E}^r = \underline{u}_r \, e^{-j\underline{k}_r \cdot \underline{r}_n} \tag{C.3}$$

and for E_θ component $\underline{u}_r$ is given by

$$\underline{u}_r = \underline{u}_{\theta_r} = \underline{u}_x \cos\theta_r \cos\phi_r + \underline{u}_y \cos\theta_r \sin\phi_r - \underline{u}_z \sin\theta_r \tag{C.4}$$

and

$$\underline{E}^i = \underline{u}_i \, e^{-j\underline{k}_i \cdot \underline{r}_n} \tag{C.5}$$

for E_θ component $\underline{u}_i$ is given by

$$\underline{u}_i = \underline{u}_{\theta_i} = \underline{u}_x \cos\theta_i \cos\phi_i + \underline{u}_y \cos\theta_i \sin\phi_i - \underline{u}_z \sin\theta_i \tag{C.6}$$

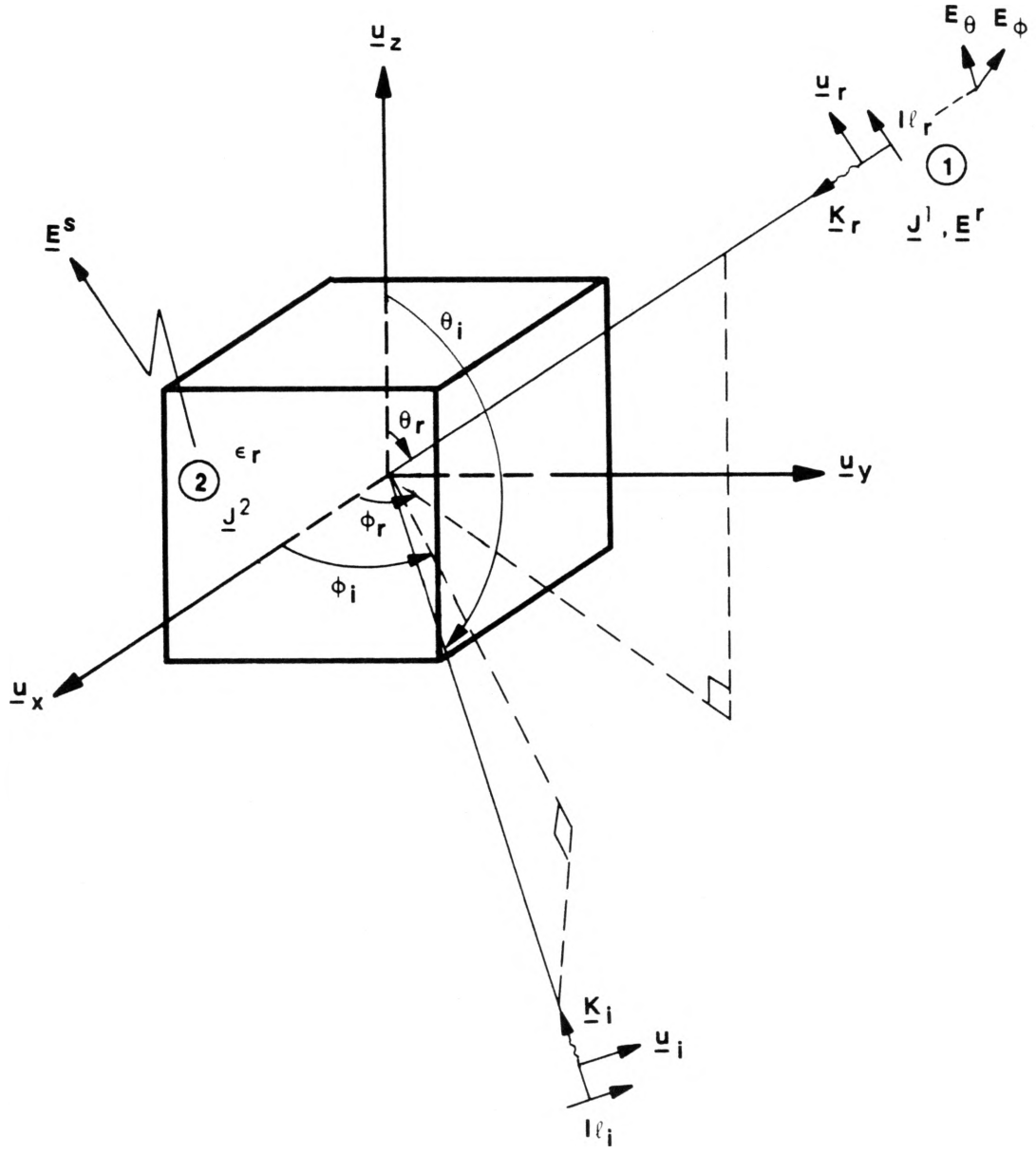

Figure C1. Three-Dimensional Coordinates for Incident and Receiving Test Dipoles in Reciprocity Relationship

in rectangular coordinates.

$\underline{E}^i$ is the incident transmitted field where $\underline{u}_r$ and $\underline{u}_i$ are the unit vectors specifing the polarization of the wave. The wave numbers $\underline{k}_r$ and $\underline{k}_i$ are pointing in the direction of travel and $\underline{r}_n$ is the radius vector to the point n on the scatterer. Moving the test dipole to infinity and using the reciprocity relationship between sources and fields at 1 and 2 as follows:

$$\int_{\ell'} \underline{J}^1 \cdot \underline{E}^s \, d\ell' = \iiint_V \underline{J}^2 \cdot \underline{E}^r \, dv'$$

$$I\ell_r \, E^s = \iiint_V \underline{J}^2 \cdot \underline{E}^r \, dv'$$

$$E^s = \frac{1}{I\ell_r} \iiint_V \underline{J}^2 \cdot \underline{E}^r \, dv \qquad \text{(C.7)}$$

where E^s is the $\underline{u}_r$ component of $\underline{E}$ for the body and $\underline{J}^2$ is the polarization current in the body. The constant $\frac{1}{I\ell_r}$ is needed to produce a plane wave of unit amplitude at the origin. Figure C2 shows the far field relationship between source and field.

In the far zone

$$|\underline{r} - \underline{r}'| \cong r - r' \cos\zeta \qquad \text{(C.8)}$$

is the phase term and

$$|\underline{r} - \underline{r}'| \cong r \qquad \text{(C.9)}$$

is the amplitude term.

The far field electric component from the dipole is

$$E_\theta = -j\omega A_\theta \qquad \text{(C.10)}$$

where the magnetic vector potential of the test dipole $I\ell_r$ is given by

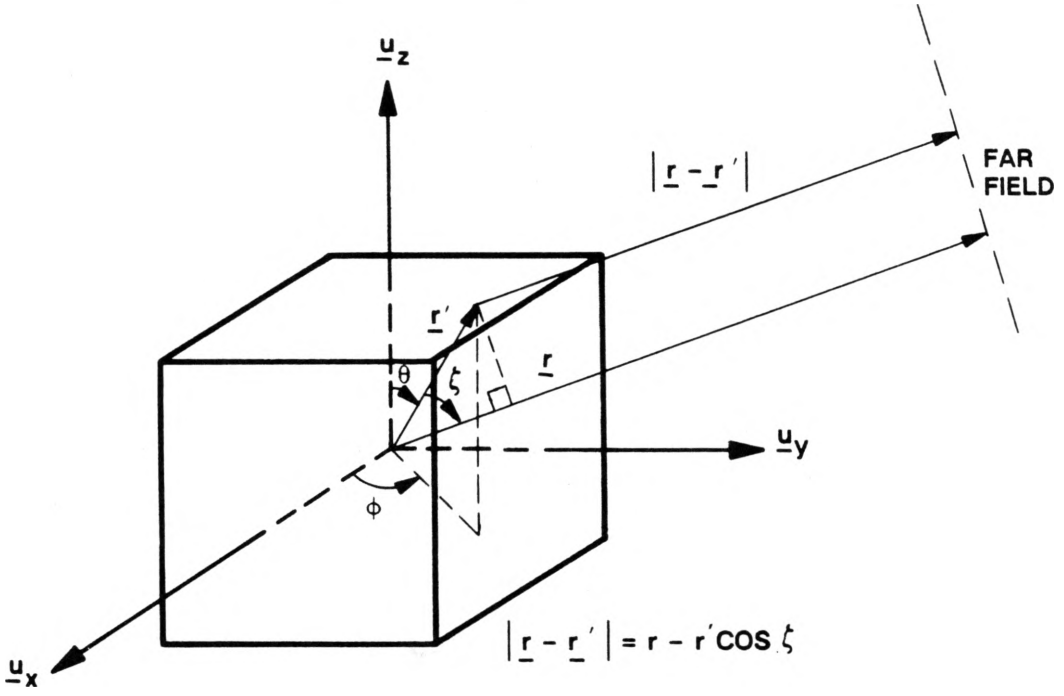

Figure C2. Coordinates for Far Field Source and Observation Point in Three Dimensions

$$A_\theta = \frac{I\ell_r \mu_o}{4\pi} \frac{e^{-jk|\underline{r} - \underline{r}'|}}{|\underline{r} - \underline{r}'|}$$

$$= \frac{I\ell_r \mu_o}{4\pi} \frac{e^{-jk(r - r'\cos\zeta)}}{r}$$

$$= \frac{I\ell_r \mu_o}{4\pi r} e^{-jkr} e^{+jkr'\cos\zeta} \qquad (C.11)$$

Substitution of (C.11) into (C.10) to solve for the far field gives

$$E_\theta = -j\omega A_\theta = \frac{-j\omega I\ell_r \mu_o}{4\pi r} e^{-jkr} e^{jkr'\cos\zeta} \qquad (C.12)$$

Setting the amplitude term to unity

$$-\frac{I\ell_r j\omega\mu_o}{4\pi r} e^{-jkr} = 1$$

$$\frac{1}{I\ell_r} = \frac{-j\omega\mu_o}{4\pi r} e^{-jkr} \qquad (C.13)$$

The scattered field is determined by substitution of (C.13) into (C.7) resulting in

$$E^s = \frac{-j\omega\mu_o}{4\pi r} e^{-jkr} \iiint_V \underline{J}^2 \cdot \underline{E}^r \, dv' \qquad (C.14)$$

A numerical approximation to the integral in (C.14) is obtained by defining a voltage receiving matrix from (3.8) as follows

$$V_m^r = \langle \underline{J}_m, \underline{E}^r \rangle$$

$$= \iiint_V \underline{J}_m \cdot \underline{E}^r \, dv' \qquad (C.15)$$

$$= \iiint_V \underline{J}_m \cdot \underline{u}_r \, e^{-j\underline{k}_r \cdot \underline{r}_n} \, dv'$$

For the one cell approximation to the cube, where the volume is centered at the origin the radius vector $\underline{r}_n$ to the evaluation point is zero therefore

$$V_m^r = \iiint_V \underline{J}_m \cdot \underline{u}_r \, dv'$$

$$= \iiint_V \underline{J}_m \cdot \left(\underline{u}_x \cos\theta_r \cos\phi_r + \underline{u}_y \cos\theta_r \sin\phi_r - \underline{u}_z \sin\theta_r \right) dv'$$

$$= \Delta^3 \underline{J}_m \cdot \left(\underline{u}_x \cos\theta_r \cos\phi_r + \underline{u}_y \cos\theta_r \sin\phi_r - \underline{u}_z \sin\theta_r \right) \qquad \text{(C.16)}$$

Substituion of $\underline{J}$ of (3.1) for $\underline{J}^2$ in (C–14) and use of (C–15) yields

$$E^s = \frac{-j\omega\mu_o}{4\pi r} e^{-jkr} \left[\tilde{V}_m^r \right] \left[I_n \right] \qquad \text{(C.17)}$$

where $[\tilde{V}_m^r]$ is the transpose of $[V_m^r]$ and $[I_n]$ is given by (3.29) with

$$V_m^i = \left\langle \underline{J}_m, \underline{E}^i \right\rangle$$

$$= \iiint_V \underline{J}_m \cdot \underline{E}^i \, dv'$$

$$= \Delta^3 \underline{J}_m \cdot \left(\underline{u}_x \cos\theta_i \cos\phi_i + \underline{u}_y \cos\theta_i \sin\phi_i - \underline{u}_z \sin\theta_i \right) \qquad \text{(C.18)}$$

Therefore (C.17) becomes

$$E^s = \frac{-j\omega\mu_o}{4\pi r} e^{-jkr} \left[\tilde{V}_m^r \right] \left[\hat{Z}_{mn}^{-1} \right] \left[V_m^i \right] \qquad \text{(C.19)}$$

Substitution (C.19) into (C.2) for bistatic radar cross section for scattering from three–dimensional bodies results in

$$\sigma_B = 4\pi r^2 \left| \frac{-j\omega\mu_o}{4\pi r} e^{-jkr} \left[\tilde{V}_m^r \right] \left[\hat{Z}_{mn}^{-1} \right] \left[V_m^i \right] \right|^2$$

$$= \frac{\eta^2 k^2}{4\pi} \left| \left[\tilde{V}_m^r \right] \left[\hat{Z}_{mn}^{-1} \right] \left[V_m^i \right] \right|^2 \qquad \text{(C.20)}$$

REFERENCES

[1] R.F. Harrington, *Field Computation by Moment Methods*, Macmillan Company, New York, 1968.

[2] M.H. Cohen, "Application of the Reaction Concept to Scattering Problems", *IRE Transactions – Antennas and Propagation*, Vol. AP–3, No. 4, pp. 193–199, October 1955.

[3] J.H. Richmond, "Scattering by a Dielectric Cylinder of Arbitrary Cross Section Shape", *IEEE Transactions on Antennas and Propagation*, Vol. AP–13, No. 3, May 1965, pp. 334–341.

[4] J.H. Richmond, "TE–Wave Scattering by a Dielectric Cylinder of Arbitrary Cross–Section Shape", *IEEE Transactions on Antennas and Propagation*, Vol. AP–14, No. 4, July 1966, pp. 460–464.

[5] D.H. Schaubert, D.R. Wilton, and A.W. Glisson, "A Tetrahedral Modeling Method for Electromagnetic Scattering by Arbitrarily Shaped Inhomogeneous Dielectric Bodies," *IEEE Transactions on Antennas and Propagation*, Vol. AP–32, No. 1, January 1984, pp.77–85.

[6] D.K. Langan and D.R. Wilton, "Numerical Solutions of TE Scattering by Inhomogeneous Two–Dimensional Composite Dielectric, Metallic Bodies of Arbitrary Cross–Section", *1986 National Radio Science Meeting Digest*, p. 91, June 1986.

[7] M.J. Povinelli, and R.F. Harrington, "A Volume Integral Formulation for Electromagnetic Scattering from Thin Dielectric Substrates", *1988 URSI Radio Science Meeting Digest*, p. 298, June 1988.

[8] R.F. Harrington, *Time–Harmonic Electromagnetic Fields*, New York: McGraw–Hill, 1961, pp. 80–81, 460–464.

[9] J.R. Reitz, F.J. Milford, and R.W. Christy, *Foundations of Electromagnetic Theory*, Reading, MA: Addison–Wesley, 1980, pp. 75–98, 80.

[10] E.C. Jordan and K.G. Balmain, *Electromagnetic Waves and Radiating Systems*, Englewood Cliffs, NJ: Prentice–Hall, 1968, pp. 300–301.

[11] R.F. Harrington, *Personal Notes*, 1987.

[12] A.W. Glisson, "On the Development of Numerical Techniques for Treating Arbitrarily–Shaped Surfaces", *PhD Dissertation*, University of Mississippi, 1978.

[13] A.W. Glisson, and D.R. Wilton, "Simple and Efficient Numerical Methods for Problems of Electromagnetic Radiation and Scattering from Surfaces", *IEEE Transactions on Antennas and Propagation*, Vol. AP–28, No. 5, pp. 593–603, September 1980.

[14] R.F. Harrington, "Matrix Methods for Field Problems", *Proceedings of the IEEE*, Vol. 55, No. 2, February 1967, pp. 136–149.

BIOGRAPHICAL DATA

Name:	Mark Joseph Povinelli
Date and Place of Birth:	August 18, 1960 Buffalo, New York
Elementary School:	St. Catherines Shreveport, Louisiana
High School:	Jesuit High School Shreveport, Louisiana
College:	University of Houston Houston, Texas B.S. 1982
Graduate Work:	Syracuse University Syracuse, New York

A VOLUME INTEGRAL FORMULATION FOR ELECTROMAGNETIC SCATTERING FROM HOMOGENEOUS DIELECTRIC BODIES

by

Mark Joseph Povinelli

B.S., University of Houston, 1982

ABSTRACT OF THESIS

Submitted in partial fulfillment of the requirements for the
degree of Master of Science in Electrical Engineering
in the Graduate School of Syracuse University
December 1988

Approved R F Harrington

Date Dec. 16, 1988

ABSTRACT

The development of a volume integral formulation for computing the electromagnetic scattering from two– and three–dimensional homogeneous dielectric bodies is presented. The two–dimensional transverse electric (TE) and three–dimensional electromagnetic scattered field is solved for numerically using a method of moments solution technique. The polarization current induced in the material body is expanded in terms of divergence–free expansion functions. These functions give rise to zero volume charge density, but produce a surface distribution of polarization charge where they have a normal component at the surface. The surface charge is related to the volume polarization current by the equation of continuity. An impedance operator in terms of integration is obtained where differentiation in the scalar potential term is avoided through use of a vector identity, the equation of continuity, and the divergence theorem. The proper choice of current and charge expansion functions assures that all improper integrals are convergent. This results in a more accurate model for determining the near fields of thin dielectric substrates required for the analysis of printed circuit antennas, scatterers, and transmission lines.

For two–dimensional problems, the expansion functions are chosen as circulating current loops for approximating the volume polarization current. When these loops terminate on the surface, they give rise to surface charge doublets. The current loops are taken to be rooftop functions combined so that the volume charge density vanishes. In two–dimensional problems, the dielectric sheet is divided into square cells, and in three–dimensional problems it is divided into cubic cells. A linearly independent set of expansion functions must be chosen to insure a non–singular impedance matrix.

The TE wave scattering solutions to a dielectric square post and a thin dielectric sheet are computed and compared to solutions obtained by a surface equivalence formulation solution, and to other numerical results. The results for electromagnetic scattering from a three–dimensional dielectric cube are also shown and compared to a surface equivalence solution. Computer programs are developed for computing the bistatic scattering cross section from a homogeneous dielectric square post, sheet, and cube.